https://doi.org/10.5194/acp-2021-1018
Preprint. Discussion started: 15 December 2021
© Author(s) 2021. CC BY 4.0 License.

Atmospheric Chemistry and Physics Discussions

Summer variability of the atmospheric NO_2:NO ratio at Dome C, on the East Antarctic Plateau

Albane Barbero[1], Joël Savarino[1], Roberto Grilli[1], Markus M. Frey[2], Camille Blouzon[1], Detlev Helmig[3], and Nicolas Caillon[1]

[1]Univ. Grenoble Alpes, CNRS, IRD, Grenoble INP (Institute of Engineering), IGE, Grenoble, France
[2]British Antarctic Survey, Cambridge, CB3 0ET, UK
[3]Boulder A.I.R. LLC, 2820 Lafayette Dr., Boulder, CO 80305, USA

Correspondence: Albane Barbero (albane.barbero@univ-grenoble-alpes.fr) and Joël Savarino (joël.savarino@cnrs.fr)

Abstract. Previous Antarctic summer campaigns have shown unexpectedly high levels of oxidants in the lower atmosphere of the continental plateau as well as at coastal regions, with atmospheric hydroxyl radical (OH) concentrations up to 4×10^6 cm^{-3}. Such high reactivity of the summer Antarctic boundary layer results in part from the emissions of nitrogen oxides ($NO_x \equiv NO + NO_2$) produced during photo-denitrification of the snowpack, but its underlying mechanisms are not yet fully understood as some of the chemical species involved (NO_2, in particular) have not yet been measured directly and accurately. To overcome this crucial lack of information, newly developed optical instruments based on absorption spectroscopy (incoherent broadband cavity enhanced absorption spectroscopy or IBBCEAS) were deployed for the first time at Dome C (-75.10 lat., 123.33 long., 3,233 m a.s.l) during the 2019–2020 summer campaign to refine uncertainties in snow-air-radiation interaction. These instruments directly measure NO_2 with a detection limit of 30 pptv (parts per trillion by volume or 10^{-12} mol mol^{-1}) (3σ). We performed two sets of measurements in December 2019 (4^{th} to 9^{th}) and January 2020 (16^{th} to 25^{th}) to capture the early and late photolytic season, respectively. Late in the season, the daily averaged NO_2:NO ratio (0.4 ± 0.4) matches that expected for photochemical equilibrium through Leighton's extended relationship involving RO_x (0.6 ± 0.3). In December, however, we observe a daily averaged NO_2:NO ratio of 1.3 ± 1.1, which is approximately twice the daily ratio of 0.7 ± 0.4 calculated for Leighton equilibrium. This suggests that more NO_2 is produced from the snowpack early in the photolytic season (December 4^{th} to 9^{th}) possibly due to stronger UV irradiance caused by a smaller solar zenith angle near the solstice. Such a high sensitivity of the NO_2:NO ratio to the sun's position is of importance for consideration in atmospheric chemistry models.

1 Introduction

Intense field campaigns over the past three decades have studied the Arctic and Antarctic boundary layer composition and photochemistry (Bauguitte et al. (2012), and references therein). The collection and interpretation of polar ice cores has led to the growing interest in the atmospheric chemistry of these regions, as well as their relatively unpolluted nature free of local anthropogenic emissions (Wolff, 1995). Antarctica, in particular, is the most isolated continent on Earth; therefore, providing the last continent scale laboratory for studying past and present natural atmospheric cycles (EPICA community members, 2004). Because of this presumed pristineness, the scientific community was puzzled by initial observations of high oxidative

https://doi.org/10.5194/acp-2021-1018
Preprint. Discussion started: 15 December 2021
© Author(s) 2021. CC BY 4.0 License.

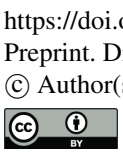

Atmospheric Chemistry and Physics Discussions

capacity in the polar boundary layer, i.e., an oxidation process initiated by oxidants, (including ozone, hydroxyl and peroxyl radicals, hydrogen peroxide, halogen radicals), which resembled those seen in urban environments (Beine et al., 2002; Mauldin et al., 2001; Davis et al., 2001; Jones et al., 2008; Kukui et al., 2014; Preunkert et al., 2012; Saiz-Lopez et al., 2008). It is today well established that such high reactivity of the summer Antarctic boundary layer results from the presence of highly reactive species, such as nitrogen oxides ($NO_y \equiv NO$, NO_2, HONO, HO_2NO_2, HNO_3 etc.), hydroxyl, and peroxyl radicals ($RO_x \equiv OH$, HO_2, RO_2), and halogen oxides ($XO \equiv BrO$, IO, ClO), due to precursor emissions from the snowpack. Despite their short lifetime and low abundance in the atmosphere, they control the oxidative capacity and the composition of the atmospheric chemistry of these regions due to their high reactivity. Today, this phenomenon is still not yet fully understood due to the difficulty of performing accurate and free of interference NO_x measurements, combined with a complex oxidation/reduction reaction involving NO_x, O_3, and radicals in the snow and atmosphere (Fig. 1).

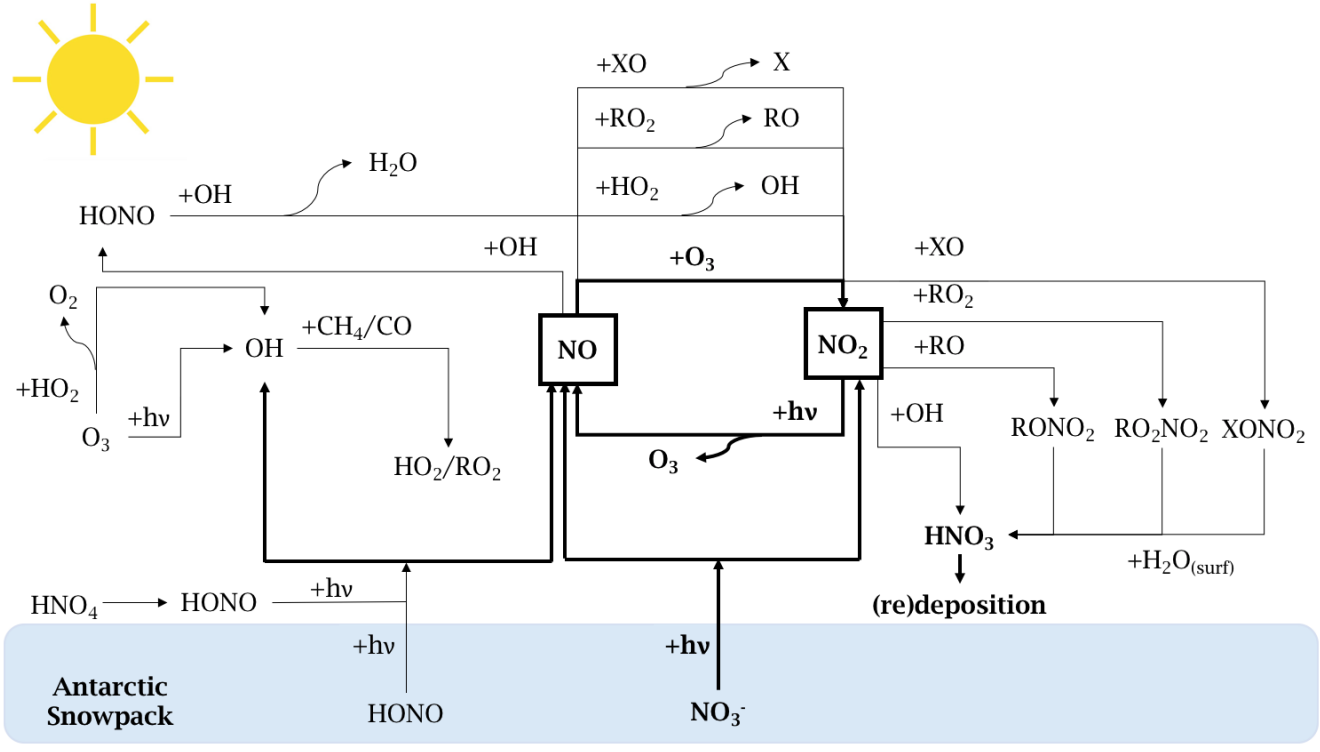

Figure 1. Schematic of the NO_x chemistry in the Antarctic Plateau. The NO_x cycle and the NO_x direct snow-sources are shown in bold.

The photolysis of nitrate ions (NO_3^-) in the snow produces NO_x ($\equiv NO_2 + NO$) (Grannas et al., 2007). Gas phase nitrogen dioxide (NO_2) photolyzes to produce nitrogen oxide (NO), which also results in production of ozone (O_3), which then reacts together to reform NO_2 (bold cycle in Fig. 1). In this recycling reaction, no net production or loss of any species is involved. However, in the presence of other species, such as peroxyl radicals (RO_x) or halogenated radicals (XO), NO can produce NO_2 without consuming O_3 (Fig. 1). NO_2 can also be consumed by reacting with hydroxyl or halogenated radicals to form

https://doi.org/10.5194/acp-2021-1018
Preprint. Discussion started: 15 December 2021
© Author(s) 2021. CC BY 4.0 License.

Atmospheric Chemistry and Physics Discussions

HNO_3, which will redeposit onto the snowpack surface. Additionally, NO can react with OH to form HONO, which was measured on the Antarctic Plateau during the OPALE campaign. HONO had been modeled to be present at around 8 to 12 pptv (parts per trillion by volume or 10^{-12} mol mol^{-1}) during the austral summer (Legrand et al., 2014). However, Legrand et al. (2014) showed that the oxidation of NO by the OH radical is not sufficient to explain the levels of HONO observed, and the main source of HONO comes from the snowpack emissions, as shown on Figure 1. The following list of campaigns and publications is not-exhaustive but gives an idea of the intensive studies of the Antarctic atmospheric chemistry for evaluating the air-snow transfer-function. ISCAT 2000 (Investigation of Sulfur Chemistry of the Antarctic Troposphere) at South Pole station in 2000 (Berresheim and Eisele, 1998; Davis et al., 2004), revealed a strong oxidizing environment at South Pole (SP), in the Antarctic Plateau. The measurements established the recycling of reactive nitrogen as a critical component of this unique environment. ANTCI (The Antarctic Tropospheric Chemistry Investigation) deployed two field studies between 2003 and 2005 with large ground-based winter-over sampling components at SP station and aircraft chemistry and photochemistry measurements (Davis et al., 2008; Eisele et al., 2008; Helmig et al., 2008; Wang et al., 2007). CHABLIS (CHemistry of the Antarctic Boundary Layer and the Interface with Snow) measurement campaign was conducted at Halley station, in coastal Antarctica, from January 2004 through February 2005 (Anderson and Bauguitte, 2007; Bauguitte et al., 2012; Bloss et al., 2007, 2010; Jones et al., 2008, 2011; Mills et al., 2007; Read et al., 2008; Saiz-Lopez et al., 2008; Salmon et al., 2008; Wolff et al., 2008). SUNITE DC (Sulfate and NItraTe surface snow Evolution at Dome C) aimed to document and use isotopic anomalies of oxyanions (sulfate and nitrate) to constrain the sources, transformations, and transports of these compounds to the polar regions where they are archived over thousands of years (Bock et al., 2016; Erbland et al., 2013; Meusinger et al., 2014; Savarino et al., 2007; Vicars and Savarino, 2014; Frey et al., 2009). OPALE (Oxidative Production over Antarctic Land and its Export) campaign took place at both coastal Antarctica (Terre Adélie, Dumont D'Urville station) and the plateau (Dome C, Concordia station), with the aim to quantify, understand, and model the level of oxidants present in the lower atmosphere of East Antarctica (Berhanu et al., 2015; Erbland et al., 2015; Frey et al., 2013, 2015; Gallée et al., 2015a, b; Kukui et al., 2014; Legrand et al., 2014, 2016; Preunkert et al., 2012, 2015; Savarino et al., 2016). Despite the numerous observations of nitrogen-bearing species, HONO, NO_x and NO, collected during those cited previous campaigns, no direct NO_2 measurements free of interferences were so far performed on the Antarctic plateau. Indeed, previous studies used chemiluminescent detectors (CLDs), which directly measure NO, and NO_y after photolytic conversion to NO, conversion subject to interferences. This absence hinders our efforts to correctly evaluate the NO_x cycle over the snowpack, leaving significant uncertainties in modeled values, which affect our full understanding of snow-air-radiation interactions. To overcome this lack of information, direct and accurate NO_2 measurements with simultaneous detection of NO are needed. Here, we deployed newly developed optical instruments in the field that allow direct measurement of NO_2 and indirect measurement of NO with detection limits of 30 and 63 pptv (3σ), respectively (Barbero et al., 2020). Although indirect, the NO measurement is well constrained. Potential artifacts have been identified and discussed in Barbero et al. (2020). Even though they may occur during night-time in an urban polluted environment, caused by the presence of N_2O_5, they are negligible during the summer period in Antarctica. We present new results on summer NO_2:NO variability over the Antarctic Plateau and explore the mechanisms involved in the atmospheric boundary layer of the Antarctic Plateau during the photolytic season in light of these new data. While the overall NO_2:NO

https://doi.org/10.5194/acp-2021-1018
Preprint. Discussion started: 15 December 2021
© Author(s) 2021. CC BY 4.0 License.

Atmospheric Chemistry and Physics Discussions

ratio can be explained by the extended Leighton's relationship, a high NO_2:NO ratio was estimated in the morning during the early photolysis season, deviating from steady state equilibrium and not explained by the extended Leighton's relationship taken from Ridley et al. (2000). Calculations show that the assumption of an additional conversion of NO to NO_2 through XO or RO_x seems insufficient to fully explain the observations. Additionally, using results of dynamic flux chamber experiments, the NO_x snow-source was better characterized highlighting that the NO_2:NO ratio is very sensitive to the position of the sun, were a 5 % difference in the solar zenith angle (SZA) between December and January may explain the equilibrium deviation observed on the NO_2:NO ratio.

2 Methods

2.1 Site Description, sampling location, and set-up

Atmospheric NO_x measurements were conducted for a total of 16 days, from 4 to 9 December 2019 and from 16 to 25 January 2020, at the French-Italian Concordia Station, Dome C, Antarctica (-75.10 lat., 123.33 long., 3,233 m a.s.l). This year-round operating station is located on the Antarctic Plateau at a distance of 1,100 km from the coast and provides an exceptional site for studying polar atmospheric chemistry. The station experiences polar night during the austral winter when the sun remains below the horizon from May to August, while in summer (November to January) the SZA has a minimum of 52°, i.e., the sun is at maximum 38° above the horizon. The local weather is generally dominated by cold, clear, and calm conditions. The annual wind speed is low due to its sitting at the top of a dome at an altitude of more than 3,200 m. Occasional regional storm systems can advect more coastal air masses associated with higher wind speeds and relatively warmer and cloudier weather (Genthon et al., 2010). The meteorological conditions encountered during the summer campaign (Fig. 2) were typical of summer climatology (November to February) observed at Dome C: T_{mean} = -29 $\pm$ 4 °C ; P_{mean} = 655 $\pm$ 4 hPa ; $W_{speed-mean}$ = 3.5 $\pm$ 1.5 m s^{-1} ; $W_{dir-mean}$ = 206 $\pm$ 71 ° ; and UV_{mean} = 24 $\pm$ 15 W m^{-2} (spectral range 305–385 nm). Five-day back-trajectories conducted by the HYSPLIT (Hybrid Single-Particle Lagrangian Integrated Trajectory) transport and dispersion model (Stein et al. (2015); Rolph et al. (2017), https://www.ready.noaa.gov) show that the air masses were principally coming from the continent during the measurement periods (more information is provided in Appendix A). The meteorological conditions encountered during both atmospheric measurement periods can be found in Appendix B.

https://doi.org/10.5194/acp-2021-1018
Preprint. Discussion started: 15 December 2021
© Author(s) 2021. CC BY 4.0 License.

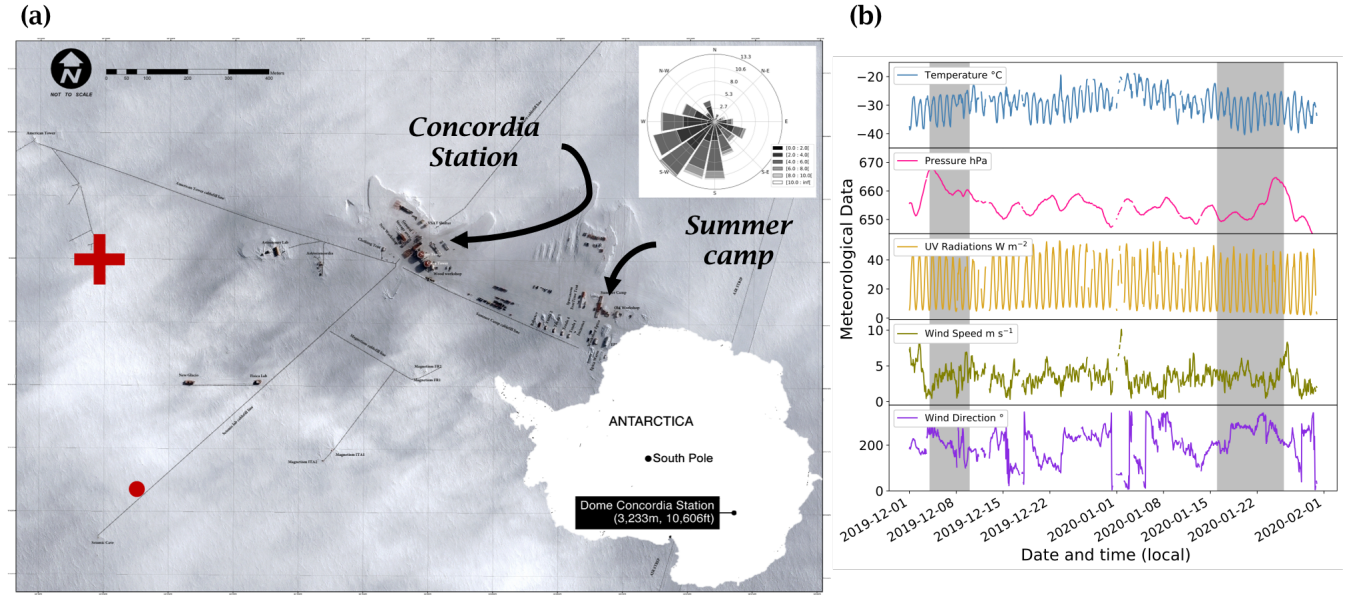

Figure 2. (a) Satellite view of the station: the red cross marks the position of the atmospheric observations and the red dot the location of the automatic weather station (AWS– Vaisala Milos 520). The wind rose for the period 01/12/2019 to 31/01/2020 is shown in the upper right-hand corner. Pléiade Satellite Image – Concordia Station, Antarctica @ CNES 2016, Distribution Airbus DS. **(b)** Local meteorological conditions (2-m observations) measured for the period 01/12/2019 to 31/01/2020 by the local automatic weather station (AWS– Vaisala Milos 520) completed with a broadband UV radiometer (spectral range 305–385 nm). The shaded areas represent the periods when atmospheric chemistry measurements were conducted.

Atmospheric sampling was done in the station's clean area sector (a zone less subject to pollution linked to the station's activities), about 1 km south-west and upwind of the main station buildings (Fig. 2). A container buried under the snow and maintained at a temperature of 8 °C was used to host the measuring instruments and all the equipment necessary for the observations (Fig. 3).

https://doi.org/10.5194/acp-2021-1018
Preprint. Discussion started: 15 December 2021
© Author(s) 2021. CC BY 4.0 License.

Atmospheric Chemistry and Physics Discussions

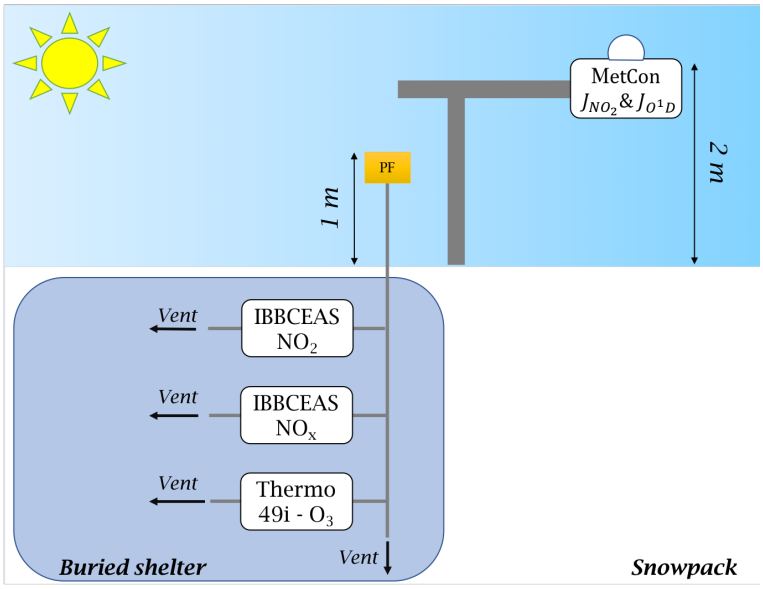

Figure 3. Set-up schematic: the photolysis rate constant of NO_2 and O^1D are measured by a 2π spectral radiometer (MetCon) placed 2 meters above the snow surface and measuring the downwelling flux, (i.e. facing the sky) ; the atmospheric sampling of NO_2, NO_x, and O_3 were made 1 meter above the snow surface through $\frac{1}{4}$" PTFE tubing. Note that 5 μm particle filters (PF) were placed at the inlets to protect the optics of the instruments measuring cells.

2.2 Instrumentation and data processing

2.2.1 Measurement of atmospheric NO_x and O_3

The twin instruments described in Barbero et al. (2020) were used for NO_x detection in the 400–475 nm wavelength region. These instruments are based on incoherent broadband cavity-enhanced absorption spectroscopy (IBBCEAS) with a high-power LED source injected in a high-finesse cavity (F ≈ 33,100), and the transmission signal is detected by a compact spectrometer equipped with a charge-coupled device (CCD) camera. Through this, we achieved direct detection of NO_2 with a detection limit of 30 pptv at 3σ precision within ≈ 20 min of measurement. To indirectly measure NO, we installed a compact ozone generator (based on water electrolysis) that converts all ambient NO into NO_2 via the reaction $NO + O_3 \longrightarrow NO_2 + O_2$. Additionally, the instrument configuration allows the spectrometer to operate at low temperature, making potential interferences from the thermal degradation of HO_2NO_2, for example, negligible (estimated at 1 pptv at 10 °C). Furthermore, very limited NO_2 (0.001 pptv) would be produced by the reaction of $HONO + OH \longrightarrow NO_2 + H_2O$ and less than 8 to 16 ppqv for 200 pptv of NO_2 would be formed through the heterogenous reaction of NO_2 and H_2O. The possible interference due to NO_2, NO or NO_3 should be limited because their rate constant is several orders of magnitudes less than that for the NO oxidation. Finally, spectral interferences were studied as small imperfections on the fit could lead to large effects on the NO_2 retrieved mixing ratio, particularly at sub-ppb levels, but no substantial effects of potential artifacts were observed when O_3 mole

https://doi.org/10.5194/acp-2021-1018
Preprint. Discussion started: 15 December 2021
© Author(s) 2021. CC BY 4.0 License.

Atmospheric Chemistry and Physics Discussions

fractions up to 8 ppmv were used, and, applied O_3 mole fractions were kept below 6 ppmv (5.6 $\pm$ 1.5 and 4.3 $\pm$ 0.5 ppmv in December and January, respectively) during this field study. Ultimate detection limits of 33 and 63 pptv (3σ) for NO_x and NO (taking into account the propagation error), respectively, are also achieved within $\approx$ 20 min of measurement (Barbero et al., 2020), according to an Allan-Werle statistical method (Werle et al., 1993). The instruments were calibrated prior and after field deployment using a stable reference NO_2 source (FlexStream™ Gas Standards Generator, KINTEK Analytical, Inc.), covering a large range of concentrations from the pptv to ppbv range (Barbero et al., 2020). In the field, a shorter time average of 10 min was used, which included the acquisition of the reference (I_0) and absorption (I) spectra. This shorter measurement still provides excellent detection limits of 54 and 48 pptv (3σ) for NO_x and NO_2, respectively, while providing a higher resolution dataset, more profitable for removing possible polluted events from the dataset. Field calibrations were made using NO_2 and NO gas bottles (Air Liquide - 1 ppm NO_2 in N_2; Messer – 1 ppm NO in N_2) diluted with a zero-air flow for multi-point calibrations. Additionally, the NO_2 bottle was calibrated prior the field campaign against the same NO_2 source as the laboratory calibrations. The zero-air was produced by pumping outdoor air through two zero-air cartridges connected in series (TEKRAN, 90-25360-00 Analyzer Zero Air Filter) and pushed into the dilution line controlled by two mass flow controllers (MKS - Mass Flow Controller at 0.01 and 10 standard liter per minute for the NO_2 flow and the zero-air flow, respectively). The NO_x measurements from the IBBCEAS were synchronized in time for a more accurate estimate of the NO mixing ratio ($NO = NO_x - NO_2$). To limit the impact of variable weather and atmospheric conditions on our NO_2 and NO observations and approximate a steady state to use Leighton's relationship (Leighton, 1961), we restricted data to when the wind was between 135° and 338° (i.e., not coming from the direction of the station) with a speed below 5 m s^{-1}. These constraints resulted in 17 % rejection rate for the first observation period and 11 % for the second period. During the second period, approximately 4 days of measurements were further rejected because the instruments were being used for intercomparison and calibration purpose. After this quality control, the accepted data observations were then aggregated to hourly means in order to reduce the sensitivity. Atmospheric ozone was monitored using a UV Photometric O_3 analyzer (Thermo Scientific™, Model 49i) that has a 1.5 ppbv (3σ) detection limit for 60 s data. The instrument was calibrated on site with an O_3 calibration source (2B Technologies Model 306 Ozone Calibration Source™) and connected to an existing air sampling tower at 1 meter above the snow surface (Helmig et al., 2020) (Appendix C). Here, samples were drawn sequentially at typical flows of $\approx$ 1-2 slpm through a series of switching valves connected to several inlet lines, following a 2-hour duty cycle of 8 minutes measurements on each inlet. To account for the switching manifold response time, only the last three minutes of measurements of steady-state concentrations were used and averaged, giving one measurement of ozone mixing ratio every 2 hours. A linear data interpolation on the O_3 measurements was applied to match the resolution of the NO_x and NO_2 measurements. Particle filters (Whatman™ PTFE membrane filters – TE 38, 5 μm, 47 mm) were placed in the inlet lines (IBBCEAS and Thermo 49i) for removing aerosol particles.

https://doi.org/10.5194/acp-2021-1018
Preprint. Discussion started: 15 December 2021
© Author(s) 2021. CC BY 4.0 License.

Atmospheric Chemistry and Physics Discussions

2.2.2 Ancillary data

Standard meteorological data were collected from an automatic weather station (AWS) located one kilometer away from the atmospheric measurements (Fig. 2). The UV radiation spectrum was analyzed with a broadband UV radiometer (Kipp & Zonen – CUV 4, spectral range 305–385 nm) deployed near the clean sector.

2.2.3 The photolysis rate coefficients J_{NO_2} and J_{O^1D}

The photolysis rate coefficients, J_{NO_2} and J_{O^1D} were calculated from measurements made by a MetCon 2π spectral radiometer with a charge coupled device. The spectral radiometer was mounted on a mast at 2 m from the snow surface on a mast (Fig. 3), and downwelling radiance was recorded over the full spectral range of the radiometer from 285 to 700 nm. Unfortunately, unstable power supply issues resulted in irregular operation during the summer campaign, particularly during local nighttime hours, and a continuous signal was reconstructed using the broadband UV radiometer to scale the data from the 2π spectral radiometer. Later, the total 4π steradian radiance was calculated by multiplying the measurements by 1.9, as this factor was determined from downwelling and upwelling radiance measurements during the OPALE campaign (Kukui et al., 2014). The estimated J_{NO_2} for both measurement periods is shown in Figure 4, and details on the fit analysis are provided in Appendix D. Due to the intermittent measurements, differences between the fit analysis and the J_{NO_2} measurements were found to be around 1 ± 7 % (1σ) in December and 4 ± 15 % (1σ) in January.

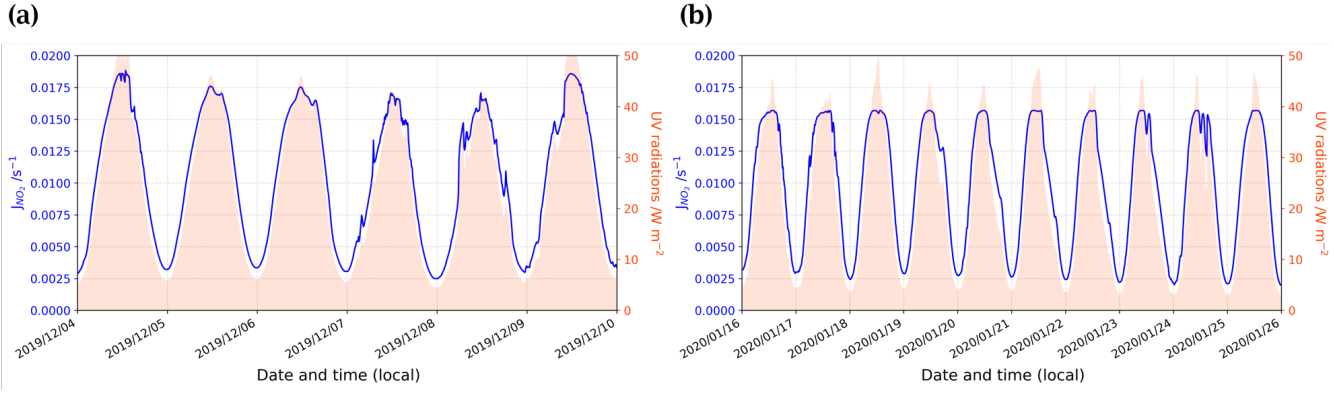

Figure 4. J_{NO_2} (blue solid lines) reconstruction following the 2 degrees polynomial regression fit (shown in Appendix D) with UV radiation (shaded orange) measured by a broadband UV radiometer (spectral range 305-385 nm) for both the December **(a)** and January **(b)** observation periods.

These extrapolations agree well with previous measurements done during the 2011-2012 OPALE campaign using the same 2π spectral radiometer. Kukui et al. (2014) found a median value of $J_{NO_2} = 1.3 \times 10^{-2}$ s^{-1} (0.4 to 2.1) from the 19/12/2011 to the 10/01/2012, very close to the one found in this work: 1.2×10^{-2} s^{-1} (0.3×10^{-2} s^{-1} to 1.9×10^{-2} s^{-1}). In a similar manner, we calculated J_{O^1D} (median value of 1.6×10^{-5} s^{-1}, range 0.2×10^{-5} s^{-1} to 5.4×10^{-5} s^{-1}) from the UV radiation data (please refer to Appendix D for more information).

https://doi.org/10.5194/acp-2021-1018
Preprint. Discussion started: 15 December 2021
© Author(s) 2021. CC BY 4.0 License.

Atmospheric Chemistry and Physics Discussions

2.3 NO_2:NO ratio analysis

If in steady state the relationship between the reactions NO + O_3 and NO_2 photolysis, known as the simple Leighton's relationship (Leighton, 1961), can be described by Equation 1:

$$NO_2 : NO = \frac{k_{NO+O_3}[O_3]}{J_{NO_2}} \quad (1)$$

with [O_3], the ozone concentration in molecules cm^{-3}; k_{NO+O_3} = 1.4 $\times$ 10^{-12} $exp(\frac{-10.89}{RT})$, the constant rate of the reaction NO + O_3 (Atkinson et al., 2004) and expressed in cm^3 molecules^{-1} s^{-1} ; and J_{NO_2}, the NO_2 photolysis rate constant in s^{-1}, measured with the MetCon instrument and reconstructed as explained in Section 2.2.3. However, as illustrated in Figure 1, the simple Leighton's relationship can be perturbed by other species such as peroxy radicals and halogenated radicals. Therefore, the NO_2:NO ratio can also be calculated from an extended Leighton mechanism also including peroxy radicals as described in Equation 2 (Ridley et al., 2000):

$$NO_2 : NO = \frac{k_{NO+O_3}[O_3] + \sum k_{NO+RO_x}[RO_x]}{J_{NO_2}} \quad (2)$$

Kukui et al. (2014) measured the RO_x at Dome C during the OPALE campaign at 1 m above the snow surface. They assumed that HO_2 and CH_3O_2 radicals represent the major part of all RO_2 radicals at Dome C, with a ratio of HO_2:RO_2 = 0.67 $\pm$ 0.05. Additionally, Kukui et al. (2014) found a linear correlation between the J_{NO_2}, measured with the same MetCon instrument, and the concentrations of RO_2 (see Figure 3 of their study). Here, we used the same correlation and the ratio of 0.67 to estimate RO_2 and HO_2 atmospheric concentrations, respectively (more information can be found in Appendix E). The reactions between those dominating peroxy radicals, RO_2 and HO_2, and nitrogen oxide are rapid with respect to NO + O_3, with mean rate coefficients of (1.10 $\pm$ 0.02) $\times$ 10^{-11} cm^3 molecules^{-1} s^{-1} and (0.91 $\pm$ 0.02) $\times$ 10^{-11} cm^3 molecules^{-1} s^{-1}, respectively, while k_{NO+O_3} = (6.35 $\pm$ 0.53) $\times$ 10^{-15} cm^3 molecules^{-1} s^{-1}, in Dome C daily conditions. Therefore, Equation 3 is used to consider those reactions and calculate NO_2:NO ratios from O_3 in-situ measurements and RO_x observations taken from Kukui et al. (2014).

$$NO_2 : NO = \frac{k_{NO+O_3}[O_3] + k_{NO+CH_3O_2}[CH_3O_2] + k_{NO+HO_2}[HO_2]}{J_{NO_2}} \quad (3)$$

2.4 Atmospheric dynamic and polar boundary layer effect

In an attempt to decipher the mechanisms occurring at Dome C during our observation periods, we decided to account for the dilution effect due to the diurnal variation of the planetary boundary layer (PBL). To do so, in the second part of the results section we referred our measurements to the total number of molecules using Equation 4 hereafter:

$$N_i = [i] \times V \quad (4)$$

with N_i, the total number of molecules of the specie i (i = NO_x, NO, NO_2, HO_2, RO_2 and O_3); [i], its concentration expressed in molecule cm^{-3}; and V, an arbitrary volume expressed as 1 cm $\times$ 1cm $\times$ H_{PBL}, with H_{PBL}, the boundary layer height in cm

https://doi.org/10.5194/acp-2021-1018
Preprint. Discussion started: 15 December 2021
© Author(s) 2021. CC BY 4.0 License.

Atmospheric Chemistry and Physics Discussions

retrieved using the MAR regional model (see Appendix F for details). This calculation assumes a homogeneous concentration distribution of the species within the PBL, an assumption supported by the flat concentration profiles observed by Frey et al. (2015) and Legrand et al. (2016) within the PBL during the OPALE campaign, where O_3 and NO_x distribution are showing homogeneous mixing ratio within the entire polar boundary layer (PBL) except from 18:00 to 00:00 Local Time (LT) due to the collapse of the convective PBL.

3 Results

Both NO_2 and NO exhibited diurnal variations, with highest concentrations in the afternoon and evening and lowest concentrations in the mid-morning to noon (Fig. 5), in association with the collapse and rise of the polar boundary layer (PBL) (Legrand et al., 2009; Frey et al., 2013, 2015). Generally, the rise and fall in NO_2 lagged behind the NO peak by 4–6 hours. As a result, the NO_2:NO ratio had less diurnal amplitude than either NO_2 or NO. Overall, the mean NO_2:NO ratio was 1.3 ± 1.1 (1σ) for December and 0.4 ± 0.4 (1σ) for January.

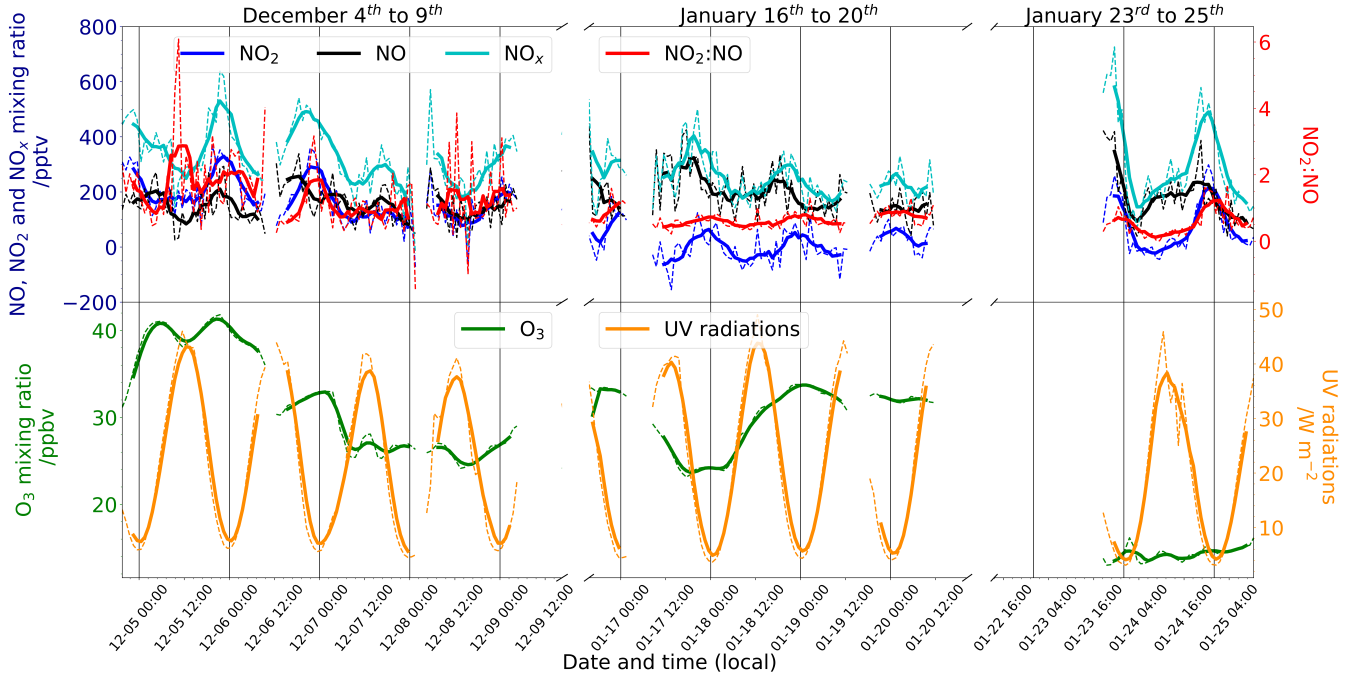

Figure 5. (top) Darkblue left-hand scale: mixing ratios (pptv) of NO_2 (blue), NO (black) and NO_x (cyan) and red right-hand scale: NO_2:NO ratio. **(bottom)** Green left-hand scale: mixing ratio of O_3 (ppbv) and orange right-hand scale: UV radiations (W m^{-2}) measured with broadband radiometer, spectral range 305-385 nm. The signals are 6-hour running means (solid) on top of one hour means signals (dashed). Each day is marked with vertical black lines at 00:00 local time (LT).

https://doi.org/10.5194/acp-2021-1018
Preprint. Discussion started: 15 December 2021
© Author(s) 2021. CC BY 4.0 License.

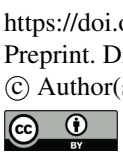

Atmospheric Chemistry and Physics Discussions

The NO_2:NO ratios calculated from the extended and simple Leighton relationships (Eq. 1, 3) share similar diurnal patterns to the observed NO_2:NO ratios, but do not reflect the difference in mean value between December and January (Fig. 6). In December, the observed NO_2:NO is systematically higher in the morning than the one estimated using simple and extended Leighton's equilibrium (Fig. 6a) while in January, it more closely matches the extended equilibrium estimations (Fig. 6b).

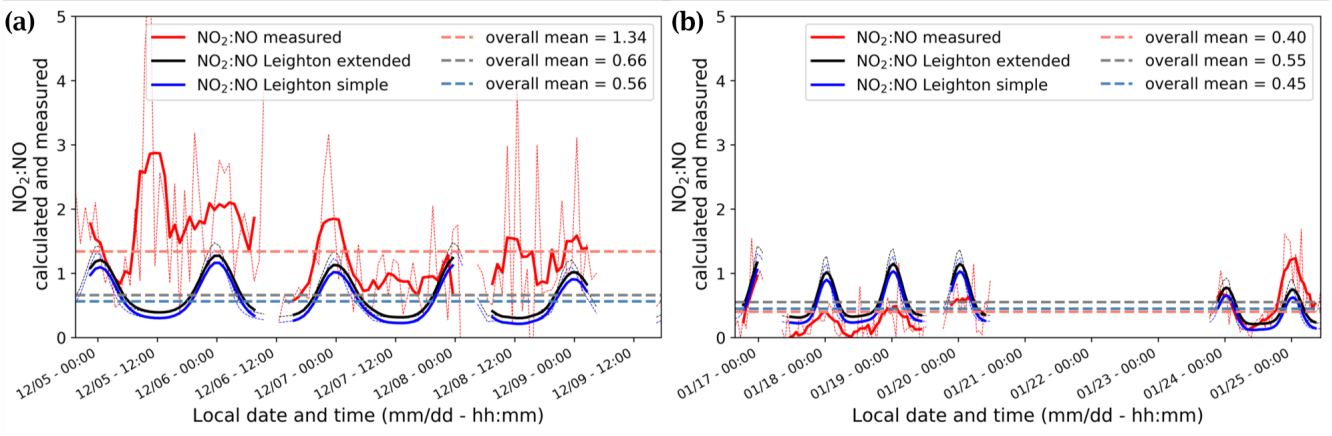

Figure 6. NO_2:NO ratios measured (red) and estimated from Eq. 1 (blue) and Eq. 3 (black) for both observation periods: December **(a)** and January **(b)**. Solid lines represent the 6-hour running mean smoothed signals.

We observed a dramatic loss of O_3 at the end of the measurement period, with the mean mixing ratio dropping from 29.8 ± 3.6 ppbv in 16–20 January to 14.3 ± 0.8 ppbv in 23–25 January. HYSPLIT 5-day backward trajectories between 14:00 and 20:00 local time (LT) on 23 January (Appendix A2) reveal that the air mass over Dome C originated from the east coast of Antarctica, and this could explain the 10 ppbv drop of O_3 observed between the two January periods shown in Figure 5. It is therefore possible that this air mass was partially affected by marine influences, as Legrand et al. (2009, 2016) concluded that O_3 mixing ratios below 20 ppbv were observed when the air masses spent at least one day above the ocean during the previous five days. As a result, we excluded the 23–25 January data from the following discussions. Top panels of Figure 7a and 7b show daily averaged of N_{NO_x} (cyan), N_{NO} (black), and N_{NO_2} (blue), total number of molecules (Eq. 4) of each species for both observation periods, December 2019 (Fig. 7a) and January 2020 (Fig. 7b) to cancel the PBL dynamic, as explained in Section 2.4. The NO_2:NO ratios observed (red) in comparison with the theoretical NO_2:NO calculated from Equation 1 (NO_2:NO simple, grey) and Equation 3 (NO_2:NO extended, black) are reported in the lower panels of Figure 7a and 7b. With the objective of testing the consistency of the observed NO_2:NO ratios with ozone production and destruction, we also reported the total number of O_3 molecules in a column of 1 cm × 1 cm × 1 H_{PBL} [cm] (green, left-hand scale), Figure 7c and 7d, with its variation over time, $\frac{d_{O_3}}{dt}$ in molecules h^{-1} (blue-gray, right-hand scale). Production of ozone, P_{O_3} [molecules h^{-1}], calculated as the NO_2 production rate from the reaction $RO_2 + NO \longrightarrow NO_2 + RO$ and $HO_2 + NO \longrightarrow NO_2 + OH$, as reported by Kukui et al. (2014), is calculated following Equation 5 and reported in violet in Figure 7c and 7d.

$$P_{O_3} = (k_{RO_2+NO}[RO_2] + k_{HO_2+NO}[HO_2]) \times [NO] \times V \quad (5)$$

https://doi.org/10.5194/acp-2021-1018
Preprint. Discussion started: 15 December 2021
© Author(s) 2021. CC BY 4.0 License.

Atmospheric Chemistry and Physics Discussions

with k_{RO_2+NO} and k_{HO_2+NO} the kinetic rate coefficients of the reactions RO_2 + NO $\longrightarrow$ NO_2 + RO and HO_2 + NO $\longrightarrow$ NO_2 + OH, respectively, expressed in cm^3 $molecules^{-1}$ s^{-1} ; [RO_2] and [HO_2], the species concentrations expressed in molecule cm^{-3} and derived from the correlation between J_{NO_2} and [RO_2] and the $\frac{[RO_2]}{[HO_2]}$ ratio (Kukui et al., 2014) ; [NO] the concentration of NO expressed in molecule cm^{-3} ; and V the arbitrary volume expressed as 1 cm $\times$ 1cm $\times$ H_{PBL} cm with H_{PBL}, given by the MAR regional model (see Appendix F for details). The overall daily mean $\frac{P_{O_3}}{V}$ calculated for this study ($\approx$ 0.22 ppbv h^{-1}) is close to the 0.3 ppbv h^{-1} calculated by Kukui et al. (2014) and to the 0.2 ppbv h^{-1} derived from the study of the ozone diurnal concentration by Legrand et al. (2009). In the lower panels of Figure 7c and 7d are reported the deviations of the observed ratio (NO_2:NO_{obs}) from the simple and extended Leighton's equilibria, ΔNO_2:NO_{sim} = NO_2:NO_{obs} - NO_2:NO_{sim} and ΔNO_2:NO_{ext} = NO_2:NO_{obs} - NO_2:NO_{ext}, for each period, respectively. Looking at Figure 7a and 7b, the NO_x, NO, and NO_2 peaks are now more in phase with the variability of the UV radiation. The total number of NO molecules and their diurnal variability appear constant from December to January with a maximum from 11:00 to 17:00 LT. NO_2 shows a similar trend in December with a maximum from 10:00 to 18:00 LT, while in January, the total number of NO_2 molecules in the atmospheric boundary layer is somewhat constant during the day, with a slight increase from 09:00 to 12:00 LT.

https://doi.org/10.5194/acp-2021-1018
Preprint. Discussion started: 15 December 2021
© Author(s) 2021. CC BY 4.0 License.

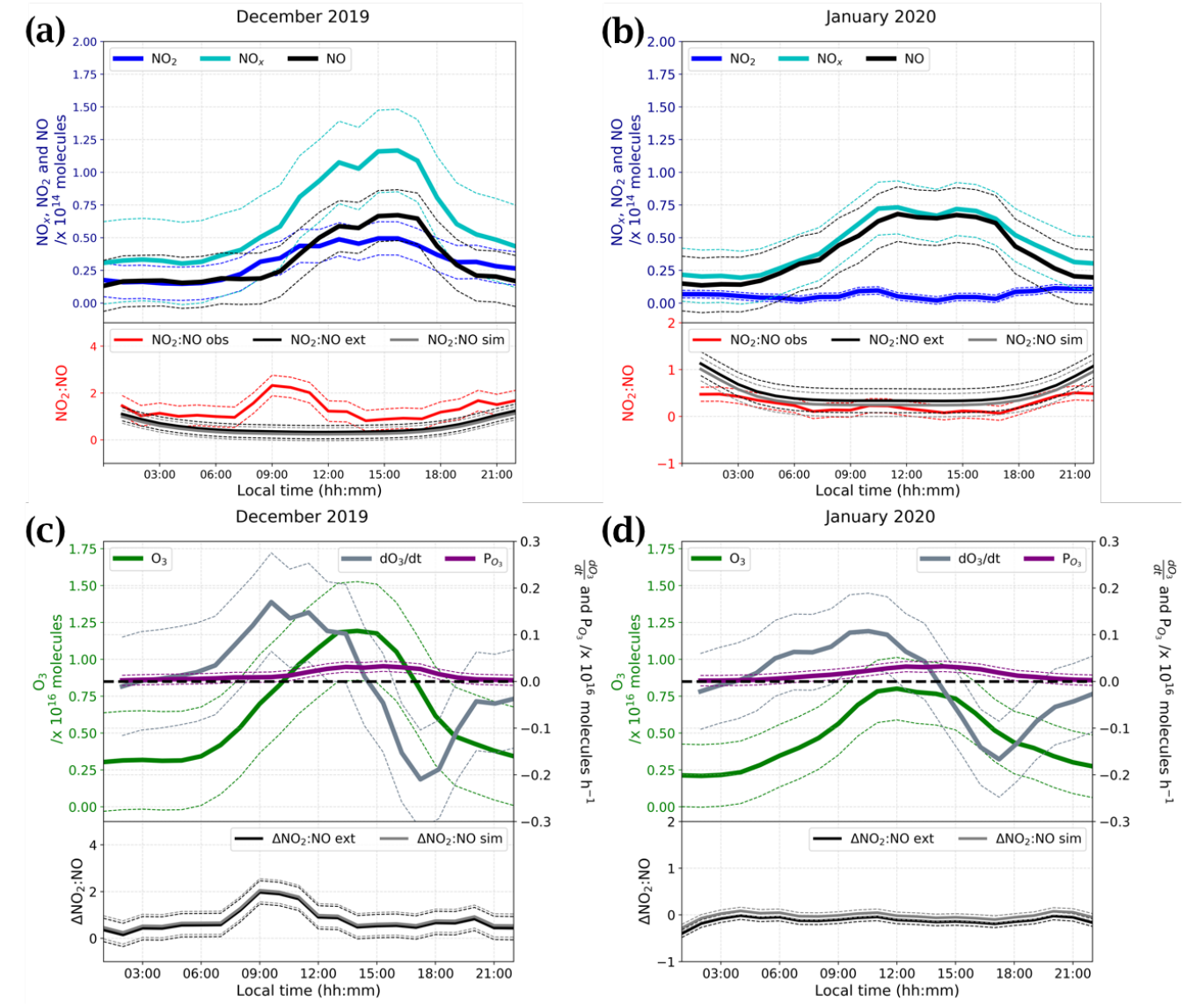

Figure 7. **(a)** and **(b)** 3-hour running mean (solid lines) $\pm$ 1σ (thin dashed lines) of the diurnal cycles of NO (black), NO_x (cyan) and NO_2 (blue) total number of molecules in a column of 1 cm $\times$ 1 cm $\times$ 1 H_{PBL} [cm] (top panels) and NO_2:NO ratios (bottom panels) observed (red) and equilibrium's calculations (simple Leighton in grey /extended Leighton in black) for December and January, respectively. **(c)** and **(d)** top panels represent the 3-hour running mean (solid lines) $\pm$ 1σ (thin dashed lines) of the diurnal cycle of the total number of ozone molecules in a column of 1 cm $\times$ 1 cm $\times$ 1 H_{PBL} [cm] (green), the O_3 variations, $\frac{d_{O_3}}{dt}$, in molecules h^{-1} (grey) and the ozone production, P_{O_3} (violet) in molecules h^{-1} calculated from the total number of RO_2 and NO molecules; the bottom panels represent the differences between NO_2:NO observed and NO_2:NO calculated, $\Delta NO_2{:}NO_{sim}$ in grey for simple Leighton and $\Delta NO_2{:}NO_{ext}$ in black for extended Leighton.

https://doi.org/10.5194/acp-2021-1018
Preprint. Discussion started: 15 December 2021
© Author(s) 2021. CC BY 4.0 License.

Atmospheric Chemistry and Physics Discussions

4 Discussion

4.1 What is driving the observed patterns?

In December, the NO_2:NO is above the NO_2:NO predicted by Leighton's equilibria (simple and extended) with a peak in the morning, from 07:00 to 12:00 LT, but approaches equilibrium from noon onwards, inversely following the ozone signal. In January, it is following quite well the equilibrium except during nighttime, when it is approximately half the predicted value calculated at steady- state. The O_3 variations measured in our study $\frac{d_{O_3}}{dt}$ show significant differences with the ozone production P_{O_3} calculated using RO_2, HO_2 and NO concentrations. P_{O_3} from Figure 7c and 7d, shows not only a factor 10 difference with the O_3 daily variations, but a rather different behavior as well. Indeed, using RO_2, HO_2 and NO concentrations, O_3 appears to be gradually produced, following the UV radiation, with a maximum production in the afternoon, from approximately 12:00 to 16:00 LT. However, this calculated production is largely insufficient to explain the observed variability of O_3. Observations show ozone production, (i.e., values above the dashed bold black line in Fig. 7), from around 02:00 to 14:00 LT, with the maximum reached at 11:00 (local solar noon) and destruction of ozone, (i.e., values under the dashed black line in Fig. 7), from 14:00 to midnight (LT), with the maximum consumption around 17:00 – 18:00 LT. While Legrand et al. (2009) attributed this behavior to the variability of the PBL, here, its impact is accounted for through the observation of a total number of molecules in a column within the boundary layer height. Therefore, the dynamic of the PBL is not the only explanation for the O_3 variability and local chemical reactions play an important role in the diurnal O_3 behavior. Even though the deviation (ΔNO_2:NO) from Leighton's equilibria is always positive, at those levels of O_3, a deviation of ΔNO_2:NO = 0.5 from steady-state might not be enough to maintain an O_3 production (Fig. 7c). Additionally, the ΔNO_2:NO peak in December is slightly shifted with respect to the $\frac{d_{O_3}}{dt}$ (Fig. 7c). This shift is explained by the chemical lifetime of the species. NO_2 lifetime, τ_{NO_2} = $\frac{1}{J_{NO_2}}$ is varying from ≈ 6 min at 00:00 LT to ≈ 1 min at 11:00 LT, largely inferior to O_3 chemical lifetime. Legrand et al. (2016) show that the main sink of O_3 is the HO_2 radical, therefore, driving its lifetime: τ_{O_3} = $\frac{1}{k_{HO_2+NO}[HO_2]}$ is varying from ≈ 2 years at 00:00 LT to ≈ 0.4 year at 11:00 LT. However, the O_3 dry deposition was not considered in the P_{O_3} calculation. The NO_2:NO ratio seems to follow Leighton's equilibrium in January and since the NO trend remains the same between the two observation periods, it highlights the necessity of an additional primary source of NO_2 other than the conversion of NO to NO_2 by reactions with O_3 and radicals as shown in Figure 1. Additionally, in January, the seemingly extended Leighton's equilibrium cannot explain the O_3 loss observed from the $\frac{d_{O_3}}{dt}$ signal. The chemical lifetime of O_3 with respect to its photolysis, τ_{O_3} = $\frac{1}{J_{O^1D}}$, J_{O^1D} reconstructed from the MetCon instrument, is estimated to be ranging from 7 hours to several days. Another sink of O_3, with chemical lifetime closer to τ_{NO_2} is necessary to explain the O_3 loss observed for both periods. In an attempt to explain the large NO_2 excess observed at maximum sunlight in December, the NO_x snow-source is studied in light of the conclusions given in Barbero et al. (2021), where Flux chambers experiments carried out from December 10^{th} to January 7^{th} during the 2019–2020 campaign at Dome C, Antarctica suggested that the photolyzable nitrate present in the snow acts as a uniform source with similar photochemical characteristics and a robust average daily photolysis rate coefficient $J_{NO_3^-}$ of (2.37 ± 0.35) × 10^{-8} s^{-1} (1σ) was estimated for the Antarctic Plateau photic zone (0–50 cm layer).

https://doi.org/10.5194/acp-2021-1018
Preprint. Discussion started: 15 December 2021
© Author(s) 2021. CC BY 4.0 License.

Atmospheric Chemistry and Physics Discussions

4.2 Comparison with previous studies

Previous studies as part of the NITEDC and OPALE missions estimated the NO_2:NO ratio at Dome C on the East Antarctic Plateau, and we can compare these estimates to our field observed data (Table 1). In this work, an average mixing ratio of 158 $\pm$ 68 pptv (1σ) was measured for NO during the December observation period, which is similar to the mixing ratios of 169 $\pm$ 115 pptv and 146 $\pm$ 63 pptv reported from the NITEDC and OPALE campaigns for a similar period (Frey et al., 2013, 2015). However, levels of NO_x and NO_2 from NITEDC and OPALE were $\approx$ 30 % greater than that measured in this study (Table 1), and as a result, their NO_2:NO ratios are similarly greater than our ratio. For January, we found an average NO mixing ratio of 188 $\pm$ 63 pptv (1σ), and this is almost 2.5 times what Frey et al. (2013) measured (80 $\pm$ 62 pptv) in January 2010. Moreover, during the OPALE campaign, Frey et al. (2015) measured $\approx$ 6 times less NO but similar NO_2 mixing ratios, leading to a high NO_2:NO of 1.7 $\pm$ 6.4 relative to our ratio of 0.3 $\pm$ 0.3. The NITEDC results suggested that either an unknown process enhancing NO_2 was taking place at Dome C, or that peroxy and other radicals would be significantly higher than elsewhere in Antarctica.

Table 1. NO, NO_2 and NO_x mixing ratios (pptv) and NO_2:NO ratios measured at Dome C during this campaign, in comparison with previous NITEDC and OPALE campaigns for similar periods (periods averages).

	December					January				
	NO (pptv)	NO_2 (pptv)	NO_x (pptv)	NO_2:NO	*Period*	NO (pptv)	NO_2 (pptv)	NO_x (pptv)	NO_2:NO	*Period*
NITEDC	169 $\pm$ 115	205 $\pm$ 107	383 $\pm$ 150	1.6 $\pm$ 1.1	10-15/12/2009[a]	80 $\pm$ 62	59 $\pm$ 41	139 $\pm$ 91	1.1 $\pm$ 1.1	15-25/01/2010[a]
OPALE	146 $\pm$ 63	259 $\pm$ 138	409 $\pm$ 194	1.8 $\pm$ 0.7	04-09/12/2011[b]	34 $\pm$ 33	64 $\pm$ 77	100 $\pm$ 108	1.7 $\pm$ 6.4	08-12/01/2012[b]
This work	158 $\pm$ 68	173 $\pm$ 85	331 $\pm$ 116	1.3 $\pm$ 1.1	04-09/12/2019	188 $\pm$ 63	43 $\pm$ 46	231 $\pm$ 62	0.3 $\pm$ 0.3	17-20/01/2020
						183 $\pm$ 82	97 $\pm$ 76	231 $\pm$ 134	0.6 $\pm$ 0.4	23-25/01/2020

[a] From Frey et al. (2013)

[b] From Frey (2021)

While differences in atmospheric dynamics and snow cover during the different campaigns could explain the discrepancy observed in December and January, where "atmospheric composition above the East Antarctic plateau depends not only on atmospheric mixing but also critically on NO_3^- concentration and availability to photolysis in surface snow as well as incident UV irradiance", as explained in Frey et al. (2015); it may also be due to different detection techniques being used. For NITEDC and OPALE (Frey et al., 2013, 2015), NO_x was measured with a 2-channel chemiluminescence detector (CLD), based on the reaction of NO with excess O_3 to produce NO_2. One channel was dedicated to NO and the other to NO_x, atmospheric NO_2 concentrations were then calculated as the signal difference between those two channels (Bauguitte et al., 2012). In our study, NO_2 is measured directly by the IBBCEAS. However, the NO measurement is made indirectly through the detection of NO_x after quantitative conversion of all ambient NO to NO_2 via NO + O_3 $\longrightarrow$ NO_2 + O_2, in a way, it is the opposite of what is done in the CLD technique. The possible interferences on NO_2 measurements from the presence of high O_3 levels are discussed in Barbero et al. (2020), as several reactions could be triggered at elevated O_3 concentrations, as discussed in Section 2.2.1. The discrepancies observed between the IBBCEAS measurements and the previous CLD measurements could be explained by

https://doi.org/10.5194/acp-2021-1018
Preprint. Discussion started: 15 December 2021
© Author(s) 2021. CC BY 4.0 License.

Atmospheric Chemistry and Physics Discussions

positive and negative interferences on the CLD technique. Indeed, the indirect measurement of NO_2 by the CLD may suffer from interferences due to the presence of other gaseous species, such as HONO and HO_2NO_2, in the inlet lines which will be then photolytically converted. Reed et al. (2016) suggested that measurements of NO_2 using CLD systems may be significantly biased in low-NO_x environments, especially in pristine environments, such as Dome C, where the NO_y to NO_x ratio may be high. The thermal decomposition of NO_y species within the NO_2 converter can produce unreasonably high measurements. Additionally, the photolytic conversion unit of the CLD instrument used in previous campaigns was at 30 °C, therefore the thermal decomposition of HO_2NO_2 could indeed be an important source of interference. Frey et al. (2013, 2015) discussed this possible interference and estimated it to 8-16 % of the average NO_2 measurement at 1 m from the snowpack. This interference might indeed partially explain the higher NO_2:NO ratio observed during previous campaigns in respect to our study.

4.3 Presence of halogenated radicals

During the OPALE campaign, bromine oxide (BrO) column amounts were measured using a ground base UV-visible spectrometer (MAX-DOAS, Roscoe et al. (2014)). After a complex analysis of the spectra, Frey et al. (2015) estimated a BrO median daily value of 2-3 pptv near the surface at Dome C. Additionally, Schönhardt et al. (2012) observed via satellite the presence of BrO and IO over Antarctica. However, the monthly maps of IO vertical column amounts (Fig. 4 of the study) show the presence of IO in the Antarctic Plateau late in spring (September-October) around 1.0 to 1.5 $\times$ 10^{12} molecules cm^{-2}. In contrast, in summer, they found a column amount of IO below the limit of detection, i.e. below 0.7 pptv once converting the column amount to volume mixing ratio (satellite observations averaged over six subsequent years 2004-2009) (Schönhardt et al., 2008). Vertical concentrations of BrO were found to be similar between December and January, ranging from 6.0 $\times$ 10^{13} to 7.0 $\times$ 10^{13} molecules cm^{-2} (Fig. 5 of the 2012 Schönhardt et al. study). To our knowledge, there are no reports of near-surface ClO measurement in Antarctica. The reactions NO + XO $\longrightarrow$ NO_2 + X (X $\equiv$ Br, I or Cl) show very similar reactions rate coefficients. Therefore, we consider here an average of all halogenated radicals XO to have a daily average rate coefficient of (2.5 $\pm$ 0.4) $\times$ 10^{-11} cm^3 molecules^{-1} s^{-1}. The necessary amount of XO to reach steady-state in December was calculated following Equation 6:

$$NO_2 : NO = \frac{k_{NO+O_3}[O_3] + k_{NO+HO_2}[HO_2] + k_{NO+CH_3O_2}[CH_3O_2] + k_{NO+XO}[XO]}{J_{NO_2}} \quad (6)$$

which is rearranged and simplified to Equation 7:

$$[XO] = \Delta NO_2 : NO \left(\frac{J_{NO_2}}{k_{NO+XO}} \right) \quad (7)$$

Daily mean average of XO of 17 pptv were estimated, with a peak of 64 pptv at 11:00 LT. If such high levels of XO were present, they would have been detected by Frey et al. (2015) MAX-DOAS as XO is suspected to be mainly BrO at Dome C. Additionally, such high levels of XO would induce a fast destruction of O_3, which was not observed either, and last, NO levels should have been lower in December than in January. Therefore, the assumption of an additional conversion of NO to NO_2 through XO or RO_x seems insufficient to explain the observations, and only the increased production of NO_2 from primary sources of NO_2 by a factor of two may justify the NO_2 excess observed in December and not in January. In the following

https://doi.org/10.5194/acp-2021-1018
Preprint. Discussion started: 15 December 2021
© Author(s) 2021. CC BY 4.0 License.

Atmospheric Chemistry and Physics Discussions

sections, the NO_x snow-source is studied in the light of the conclusions of Barbero et al. (2021), where dynamic flux chamber experiments allowed a new parameterization of the snow nitrate photolysis occurring at Dome C.

4.4 NO_2 snow source

In Barbero et al. (2021), results of dynamic flux chamber experiments deployed on the Antarctic Plateau at Dome C are presented. A nitrate daily average photolysis rate constant, $J_{NO_3^-}$ = (2.37 ± 0.35) × 10^{-8} s^{-1} for all different snow samples (depth and location) of the Antarctic Plateau (from the 10^{th} of December to the 07^{th} of January) is estimated. In the light of this new estimate, the NO_x snow-source is studied here to evaluate the NO_x fluxes, F_{NO_x} and NO_x production rate, P_{NO_x} in December and January using Equation 8:

$$F_{NO_x} = \int_z^0 J_{NO_3^-}[NO_3^-]dz \tag{8}$$

with $[NO_3^-]$ the concentration of nitrate in molecules cm^{-3} of snow available in the photic zone, defined as z = -50 cm (Erbland et al., 2013).

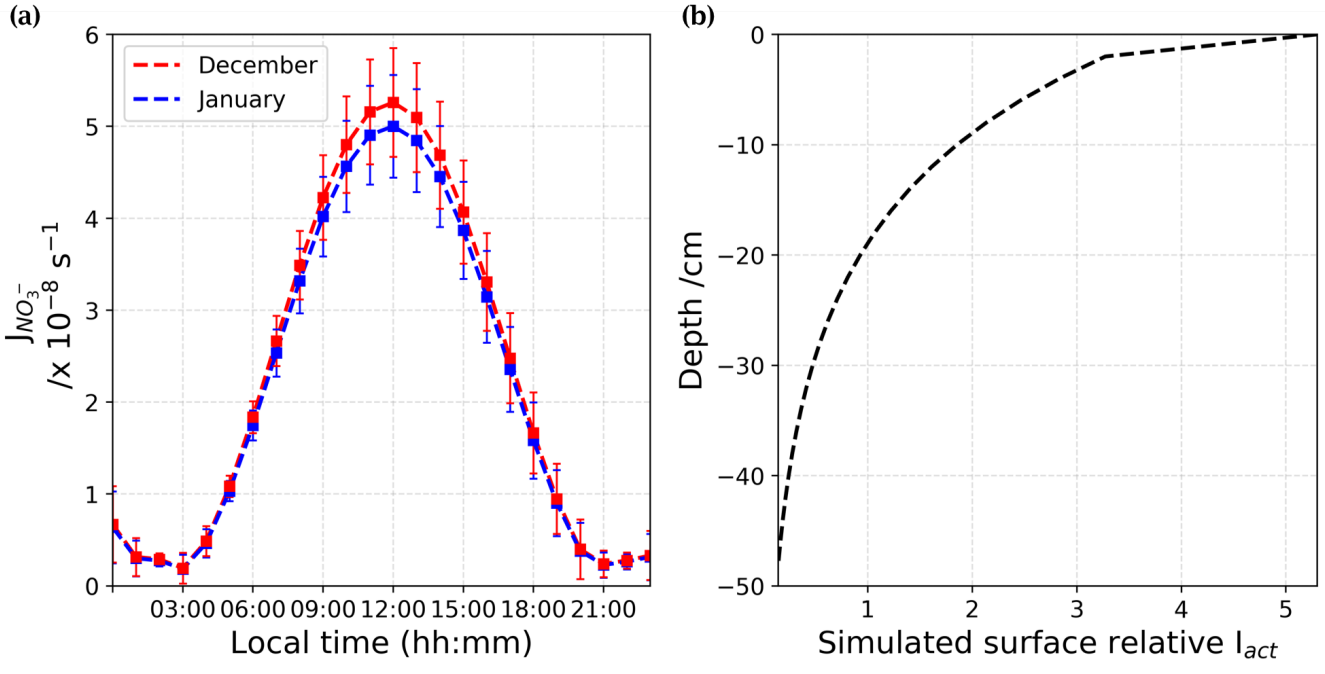

Figure 8. (a) Adjusted $J_{NO_3^-}$ [s^{-1}] from December (red) and January (blue) estimated from Barbero et al. (2021), results. **(b)** Mean surface relative actinic flux, I_{act}, profile at 305 nm, calculated using the TARTES model (Libois et al., 2013, 2014). The actinic flux describes the number of photons incident at a point.

https://doi.org/10.5194/acp-2021-1018
Preprint. Discussion started: 15 December 2021
© Author(s) 2021. CC BY 4.0 License.

Atmospheric Chemistry and Physics Discussions

The nitrate photolysis rate coefficients were adjusted for the SZA variations, and corrective factors of 0.987 and 0.938 were found for December and January, respectively. At maximum sunlight, the $J_{NO_3^-}$ is slightly lower in January than in December as the greater SZA in January lowers the maximum peak of UV radiation (Fig. 8a). Figure 8b shows the mean surface relative I_{act} profile over the photic zone extracted from the SBDART model, Libois et al. (2013, 2014), at 305 nm, the optimal wavelength for nitrate photolysis. The attenuation of $J_{NO_3^-}$ in the photic zone is driven by the attenuation of the $I_{act}(\lambda,\theta,z)$ as shown by Equation 9:

$$J_{NO_3^-}(\lambda) = \int_z^0 \sigma_{NO_3^-}(\lambda,T)\phi(T,pH)I_{act}(\lambda,\theta,z)dz \tag{9}$$

where θ is the SZA ; λ [nm] is the wavelength ; and z [m] is the snowpack's depth ; $\sigma_{NO_3^-}(\lambda,T)$ is the absorption cross-section of nitrate ; $\phi(T,pH)$ and $I_{act}(\lambda,\theta,z)$ are nitrate photolysis quantum yield and actinic flux, respectively.

4.4.1 Surface snow

From Figure 8b, one can see that I_{act} attenuates quickly with depth in the snowpack following an exponential decrease. Thus, the first few millimeters of the snow column dominate the availability of photons for photochemical reactions in the UV. Nitrate concentration measurements on surface snow were performed on a regular basis and for several years at Dome C (NITEDC and CAPOXI programs). To reduce spatial and temporal variability, average surface concentration for periods corresponding to our atmospheric observations from samples taken at different locations in the clean area sector are used. The average nitrate concentration in surface snow (few mm) is 991 $\pm$ 341 ppbw (parts per billion by weight or ng g^{-1} of snow) (median 931 - 70 samples) in December and 588 $\pm$ 248 ppbw (median 558 - 65 samples) in January, respectively. This $\approx$ 40 % difference between December and January at the surface of the snowpack is significantly large. Considering Equation 8 with a negligible dz for surface snow samples, we estimated the NO$_x$ fluxes [molecules cm^{-2} s^{-1}] from the snow surface source and converted it into a production rate in molecules cm^{-3} h^{-1} using the PBL height (cm). This production was then converted into pptv h^{-1} using atmospheric pressure, P [hPa], and temperature, T [K]. Additionally, the mean surface relative I_{act} profile shows an enhancement of the actinic flux in the very first mm of snow (Fig 8b), therefore, we multiplied the results by an enhancement factor of 5. Figure 9 pictures the estimated P_{NO_x} [pptv h^{-1}] from the surface snow for both periods. Because of the difference in nitrate in the surface snow, we estimated a mean ratio of 1.92 $\pm$ 0.33 in the NO$_x$ production between December and January (Fig. 9 - black curve on the right-hand scale). It is worth noticing that factor up to 2.6 in the surface snow NO$_x$ production between December and January could be reached in the early morning.

https://doi.org/10.5194/acp-2021-1018
Preprint. Discussion started: 15 December 2021
© Author(s) 2021. CC BY 4.0 License.

Atmospheric Chemistry and Physics Discussions

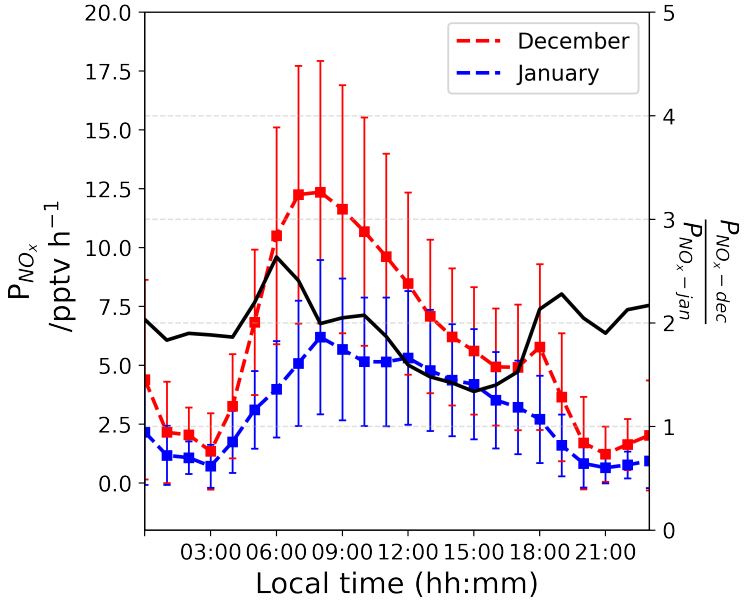

Figure 9. Left-hand scale: Estimated P_{NO_x} [pptv h^{-1}] in a column of 1 cm × 1 cm × H_{PBL} cm from December (red) and January (blue). Right-hand scale, their ratio $\frac{P_{NO_x-Dec}}{P_{NO_x-Jan}}$ (unitless).

4.4.2 Snowpack

An automatic snow tower experiment (Helmig et al., 2020), allows continuous year-round NO_x and O_3 measurements at
370 different snow depths and heights above the snow surface, and this monitoring has been maintained since 2015 at the same location as our atmospheric observations (more information in Appendix C). However, due to technical problem with the NO_x analyzer during the 2019-2020 campaign, only the O_3 monitoring instrument was running. Figure 10 shows averaged 24 h NO_x mixing ratios in the interstitial air at -48 cm recorded in 2016-2017 for similar periods of time.

https://doi.org/10.5194/acp-2021-1018
Preprint. Discussion started: 15 December 2021
© Author(s) 2021. CC BY 4.0 License.

Atmospheric Chemistry and Physics Discussions

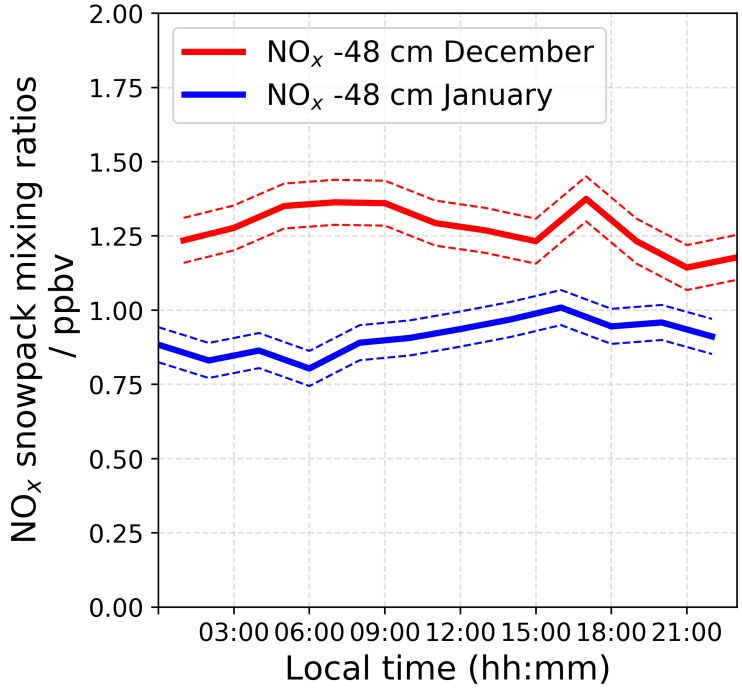

Figure 10. Averaged 24 h NO_x mixing ratios measured in the interstitial air at -48 cm by the automatic snow tower experiment in 2016-2017 for similar periods as our atmospheric observations.

One can see that the NO_x measured at -48 cm, the bottom part of the photic zone, is ≈ 50 % times higher in December 2016 than in January 2017, strengthening the theory of a strong variability in the NO_x snow-source during the photolytic season, with a depleted NO_x reservoir toward the end of the light season. It is worth noticing that the NO_3^- profiles are similar between the two seasons. Additionally, calculations based on the FC results are probably underestimating the actual NO_x snow-source, as mentioned in Barbero et al. (2021). Indeed, as discussed in Frey et al. (2013), the observed night time increase in wind shear at Dome C (Fig. 2) likely causes enhanced upward ventilation of NO_x that temporarily accumulated in the upper snow pack during very stable conditions. This analysis is strengthening the hypothesis of an enhanced NO_2 snow-source in December, when the additional NO_2 flux seems sufficient to explain the NO_2 surplus.

However, additional investigations on possible unidentified mechanisms or sinks of O_3, are needed. Indeed, if the NO_x snow-source might explain the differences between December and January in the NO_x cycle, this does not support the observed O_3 variations. Halogenated radicals, such as iodine (IO) and bromine (BrO) probably play their part, although not significantly observed on the nitrogen oxides signal, but possibly explaining the behavior of the ozone signal. Indeed, very recently, Spolaor et al. (2021), observed a continuous decline since the 70s in the iodine concentration in ice-core samples from inner Antarctica. The study states that the enhanced UV radiation caused by the stratospheric ozone hole results in the increase of iodine re-

https://doi.org/10.5194/acp-2021-1018
Preprint. Discussion started: 15 December 2021
© Author(s) 2021. CC BY 4.0 License.

Atmospheric Chemistry and Physics Discussions

emissions from the snowpack. This ice-to-atmosphere iodine mass transfer could indeed explain the ozone behavior observed in the work presented here, as iodine catalytic cycles play a crucial role in the destruction of tropospheric ozone.

5 High sensitivity of the NO_2:NO ratio to the sun's position

A possible reason to this productivity of the snowpack in the morning during the earlier phase of the photolysis season is the number of photons available, leading to higher rate of photolysis in December. Nitrate photolysis in snow occurs for wavelengths $\lambda > 300$ nm (305 nm being the optimal wavelength). Measurements of solar UV spectral radiation have been continuously recorded at Concordia since 2007 as part of the Network for the Detection of Atmospheric Composition Change (NDACC). The instrument, SAOZ (Système d'Analyse par Observation Zenithal) is an $UV - Visible$ (310-650 nm) diode array spectrometer, (1 nm resolution), looking at the scattered sunlight (Pommereau and Goutail, 1988; Kuttippurath et al., 2010).

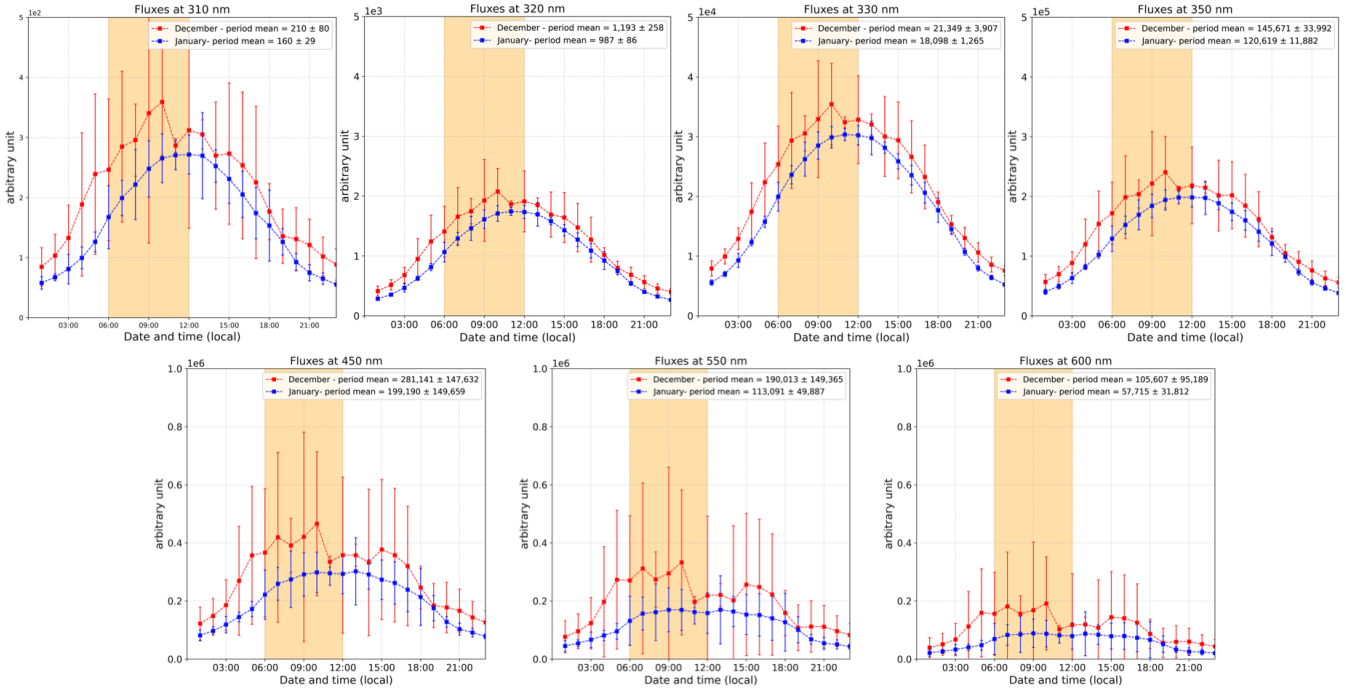

Figure 11. 2-hour running $\pm$ 1σ (error bars) of the period averaged diurnal cycles of relative radiation fluxes at different wavelengths (310, 320, 330, 350, 450, 550, and 600 nm) for both period (December and January). The yellow shaded area corresponds to the period where the NO_2:NO ratio is deviating from the steady-state equilibrium in December.

Figure 11 shows the relative radiation fluxes at different wavelengths in arbitrary unit. One can see that the relative radiation flux is systematically higher in December than in January, which could be expected as 18 days separate the first observation period to the summer solstice against 27 days for the second period. While this explains higher levels of NO_x due to more

https://doi.org/10.5194/acp-2021-1018
Preprint. Discussion started: 15 December 2021
© Author(s) 2021. CC BY 4.0 License.

Atmospheric Chemistry and Physics Discussions

photolysis activity in the snowpack in December than in January, it does not explain the early morning excess. Indeed, one can see in Figure 11 that the diurnal cycle of the radiation is somewhat symmetrical in January (in blue), while an asymmetry appears in December (in red). This is also visible while comparing the shape of the SZA for the two periods, with the difference between the two SZA cycles (black line in Figure 12), showing a bump in the morning between 06:00 and 12:00 with similar shape as the NO_2:NO deviation from equilibrium reported in Figure 7a. No different cloud cover during the two observation windows was experienced, therefore, the discontinuity in the sinusoidal shape of the radiation signal in December could be due to a smaller solar zenith angle at this latitude. Indeed, as shown in Figure 12, the difference between the SZA in January and in December, $\Delta(SZA_{jan} - SZA_{dec})$ normalized to the December value to get percentages (black line Fig. 12), appears, indeed, higher (close to 5 %) in the morning, than during the rest of the day coinciding with the bump of UV and the NO_2:NO equilibrium deviation observed before.

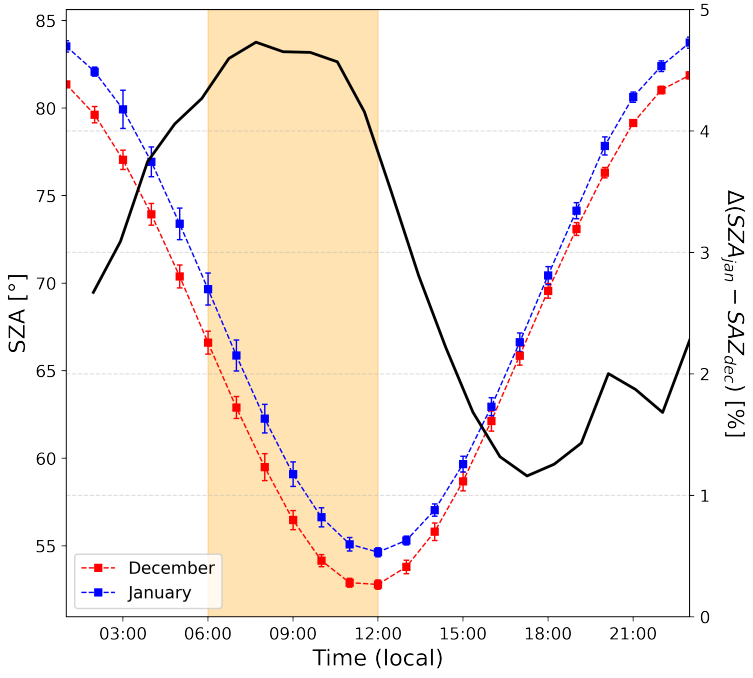

Figure 12. (left-hand scale) 2-hour running $\pm$ 1σ (error bars) of the period averaged diurnal cycles of SZA (Solar Zenith Angle) for both periods (December and January). The yellow shaded area corresponds to the period where the NO_2:NO ratio is deviating from the steady-state equilibrium in December. **(right-hand scale)** % difference between SZA in January and in December, normalized to the December value.

A rapid parameterization of the dependence of the NO_x production, P_{NO_x} [pptv h^{-1}], to the position of the sun, SZA [°], has been established, taking as reference the SZA in December and keeping only the daily values (06:00 to 18:00 LT). Figure 13 shows the results of linear regressions for both periods, suggesting that it is possible to decipher the parameters linking the NO_x production to the SZA. Indeed, satisfactory R^2 (0.984 – December ; 0.727 - January) were found. Of course, this result

https://doi.org/10.5194/acp-2021-1018
Preprint. Discussion started: 15 December 2021
© Author(s) 2021. CC BY 4.0 License.

Atmospheric Chemistry and Physics Discussions

is only an approach and a thorough study of the NO_x production dependence to the sun's position would allow to improve existing models and reduce the uncertainties concerning the Antarctic nitrogen budget.

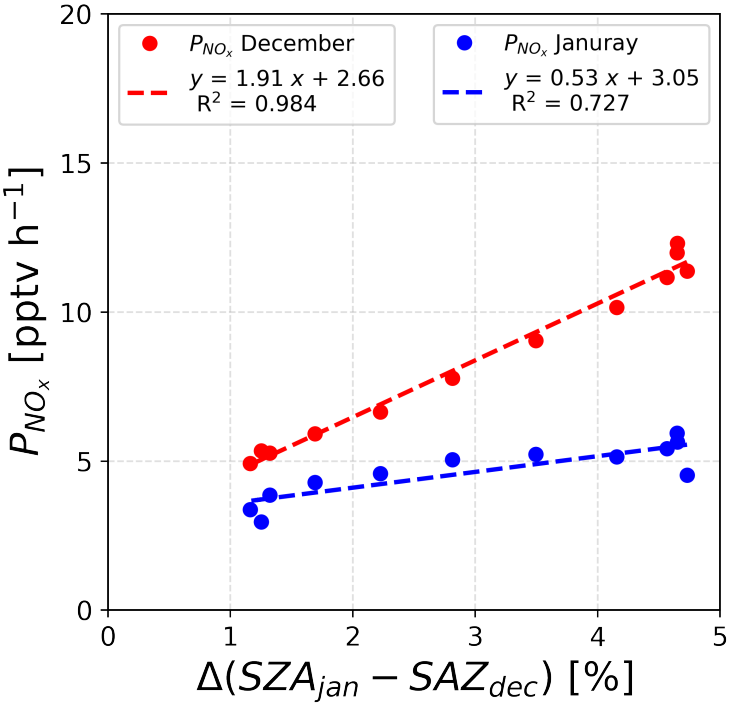

Figure 13. Correlations between the NO_x production and the $\Delta(SZA_{jan} - SZA_{dec})$ normalized to the December value for both periods of atmospheric observations.

6 Conclusions

For the first time, direct and in-situ atmospheric measurements of NO_2 were carried out in the Antarctic Plateau at Dome C. The summer variability of the NO_2:NO ratio was studied in light of this new set of observations. While the overall NO_2:NO ratio can be explained by the extended Leighton's relationship, a high NO_2:NO ratio was estimated in the morning during the early photolysis season, deviating from steady state equilibrium and not explained by the extended Leighton's relationship. The results of this study disagree with previous studies that found a systematic deviation from equilibrium, requiring around 50 pptv of halogenated radicals to explain such NO_2:NO ratio. However, the required levels of halogenated species were never observed at Dome C. While differences in atmospheric dynamics and snow cover during the different campaigns could explain the discrepancies with previous studies, it may also be due to different detection techniques being used. In our study, NO_2 was measured directly for the first time at Dome C. Evaluation of the meteorological conditions and estimation of the NO_x snow-source tend to identify the NO_x snow source and the position of the sun, through SZA measurement, as the main actors of the atmospheric oxidative capacity in the Austral summer at Dome C. Indeed, it appears that a 5 % difference on the SZA

https://doi.org/10.5194/acp-2021-1018
Preprint. Discussion started: 15 December 2021
© Author(s) 2021. CC BY 4.0 License.

Atmospheric Chemistry and Physics Discussions

in the morning could lead to an excess up to 5 times the NO_2:NO ratio when at steady state. Such a high sensitivity of the NO_2:NO ratio to the sun position is of importance to the atmospheric chemistry models, where such a parameter can be better adjusted in the future. However, if the NO_x snow-source might explain the differences between December and January in the NO_x cycle, this does not match the observed O_3 variations. Even though the depletion of the NO_x reservoir throughout the light season might explain the lower levels of O_3 toward the end of the photolytic season, additional investigations on possible unidentified mechanisms or unidentified sinks of O_3, are needed to understand the O_3 consumption. The link between the stratospheric ozone hole inducing an enhancement in the incident UV radiation, causing in return an increase in the ice-to-atmosphere iodine emissions has been established by Spolaor et al. (2021). Therefore, additional field campaigns targeting halogenated radicals' measurements in snow and troposphere in Antarctica are strongly needed in the near future to allow the scientific community to fully understand the mechanisms driving the oxidative capacity of the polar atmosphere.

Appendix A: NOAA HYSPLIT backward trajectories reconstruction for the observation periods (Dome C is represented by the black star)

Using the HYSPLIT model, 5 days (120 hours) backward trajectories were conducted. For each, day of observation, 4 runs at different times (UTC): 00:00, 06:00, 12:00 and 18:00, therefore corresponding to 08:00, 14:00, 20:00 and 02:00 (day+1) local time (LT), at different altitudes: 3,200 a.m.s.l (above mean sea level); 3,400 a.m.s.l and 3,800 a.m.s.l.

A1 December

As mentioned in Section 2.1 of the manuscript, the meteorological conditions and air masses origins in December were favorable for atmospheric measurements for the purpose of our study. Indeed, one can see on Figure A1 that the air masses were originating from the Plateau during the observation period. The 9^{th} of December at 14:00 LT, i.e., 06:00 UTC, air masses at 3,800 a.m.s.l was simulated to be originating from the Antarctic Peninsula, but this had no impact on our observations as we stopped them around 10:00 LT.

https://doi.org/10.5194/acp-2021-1018
Preprint. Discussion started: 15 December 2021
© Author(s) 2021. CC BY 4.0 License.

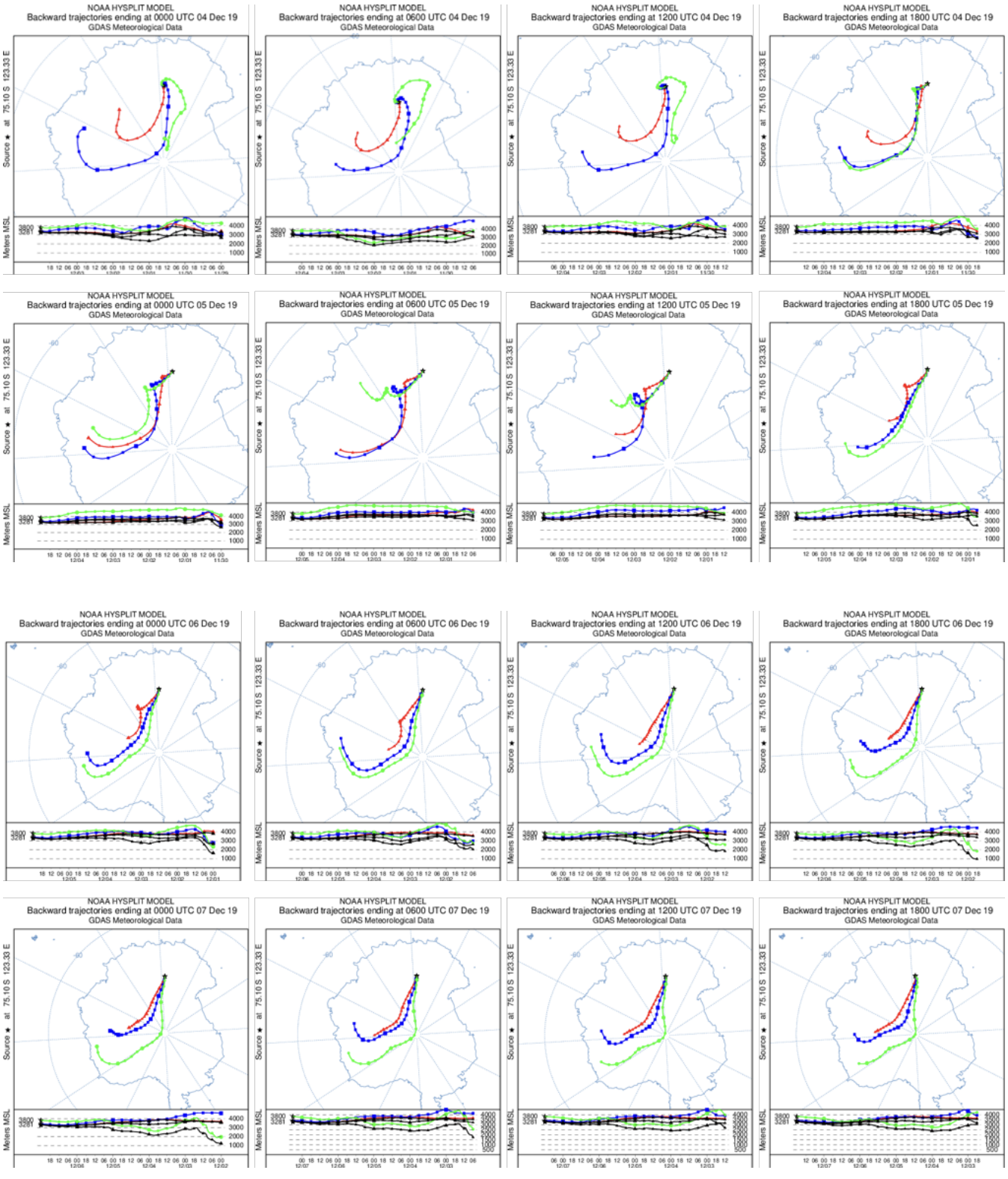

https://doi.org/10.5194/acp-2021-1018
Preprint. Discussion started: 15 December 2021
© Author(s) 2021. CC BY 4.0 License.

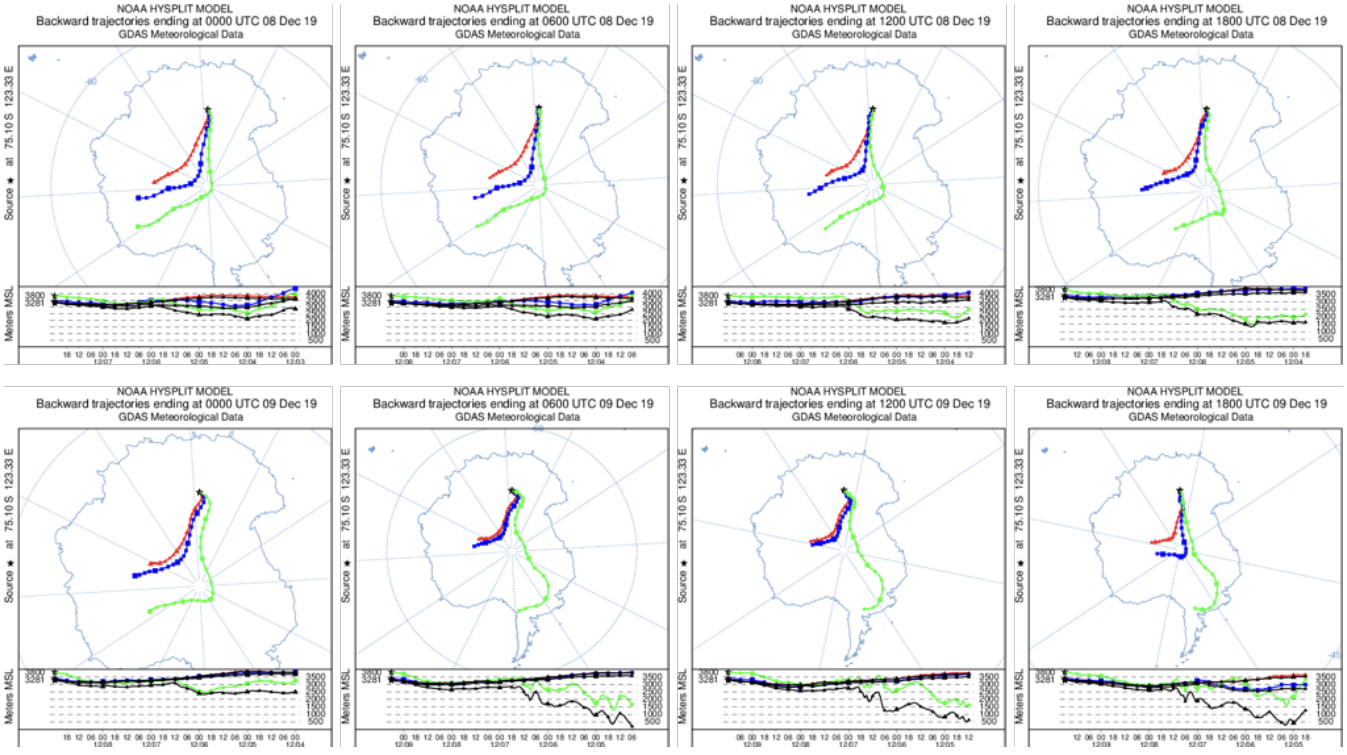

Figure A1. HYSPLIT 5 days backward trajectories from the 4^{th} to the 9^{th} of December 2019. The model was run every 6 hours for each day and at 3 different altitudes: 3,800 a.m.s.l (green), 3,400 a.m.s.l (blue) and 3,200 a.m.s.l (red).

https://doi.org/10.5194/acp-2021-1018
Preprint. Discussion started: 15 December 2021
© Author(s) 2021. CC BY 4.0 License.

Atmospheric Chemistry and Physics Discussions

A2 January

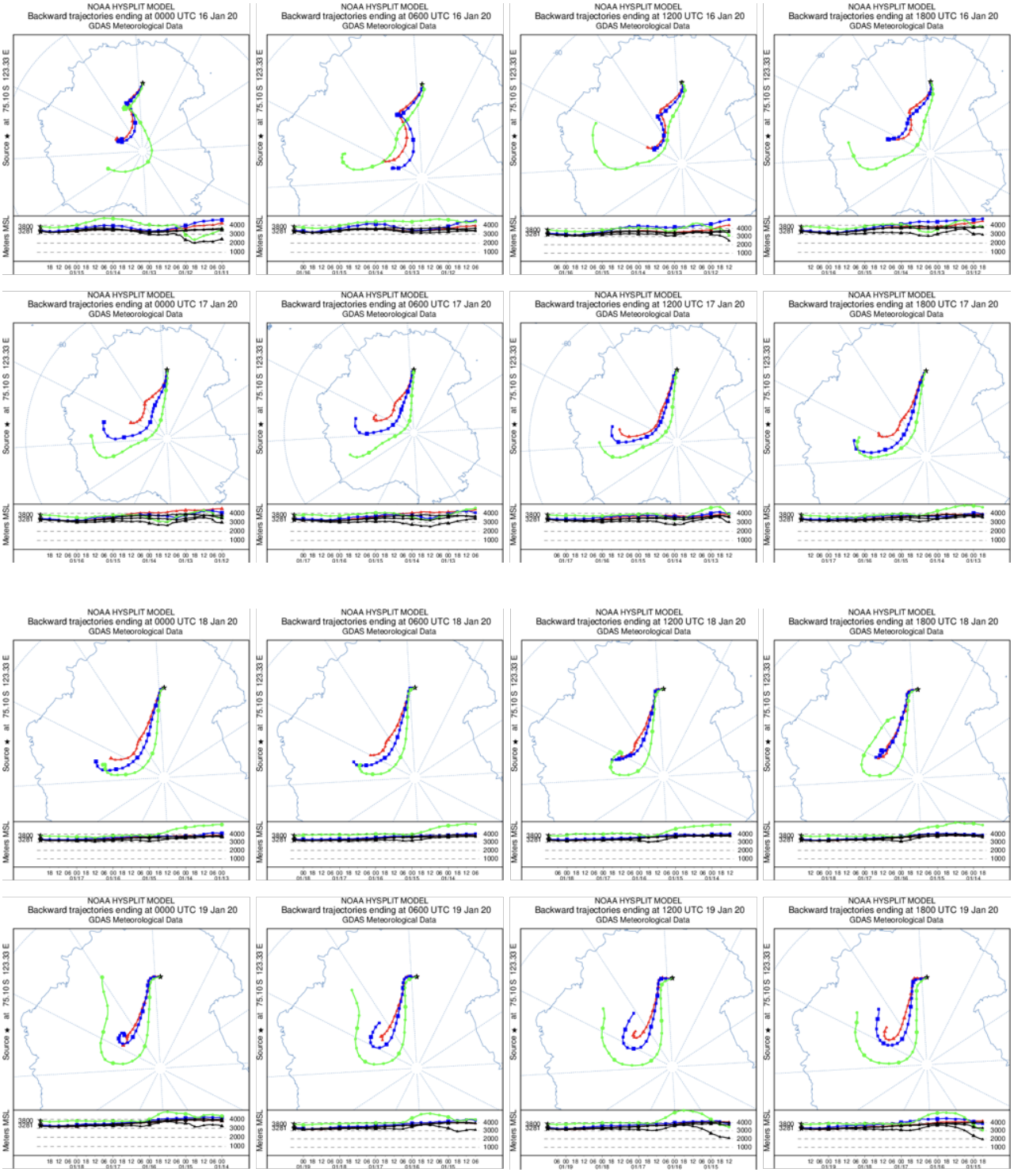

https://doi.org/10.5194/acp-2021-1018
Preprint. Discussion started: 15 December 2021
© Author(s) 2021. CC BY 4.0 License.

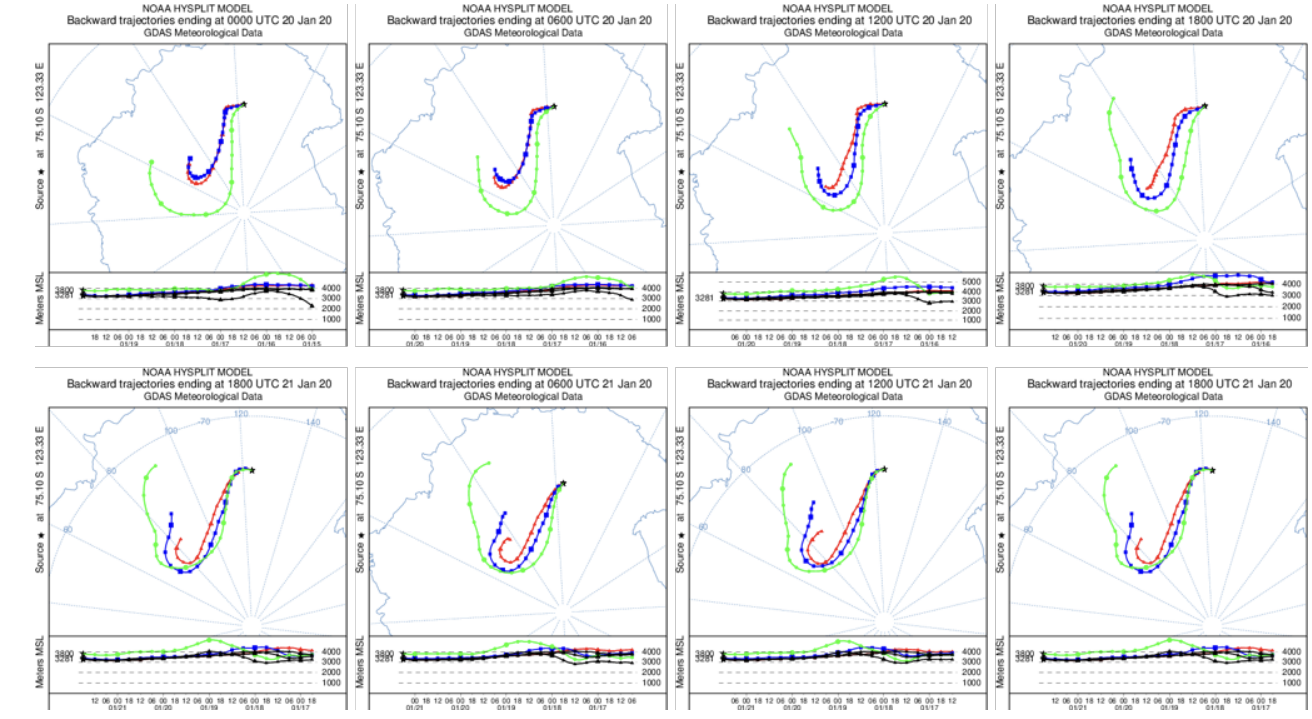

Figure A2. HYSPLIT 5 days backward trajectories from the 16^{th} to the 21^{st} of January 2020. The model was run every 6 hours for each day and at 3 different altitudes: 3,800 a.m.s.l (green), 3,400 a.m.s.l (blue) and 3,200 a.m.s.l (red).

As mentioned in Section 2.1, the meteorological conditions and air masses origins in January were favorable for atmospheric measurements from the 17^{th} to the 20^{th} of January (Fig. A2). However, the 10 ppbv drop of O_3 observed at the end of the observation period is suspected to be caused by oceanic inputs as suggested by Legrand et al. (2009). On Figure A3, a drastic change in the origin of the air masses is observed the 23^{rd} between 06:00 (UTC) and 12:00 (UTC), or 14:00 and 20:00 LT, corresponding to the sudden drop in O_3 mixing ratio around 17:00-18:00 LT.

https://doi.org/10.5194/acp-2021-1018
Preprint. Discussion started: 15 December 2021
© Author(s) 2021. CC BY 4.0 License.

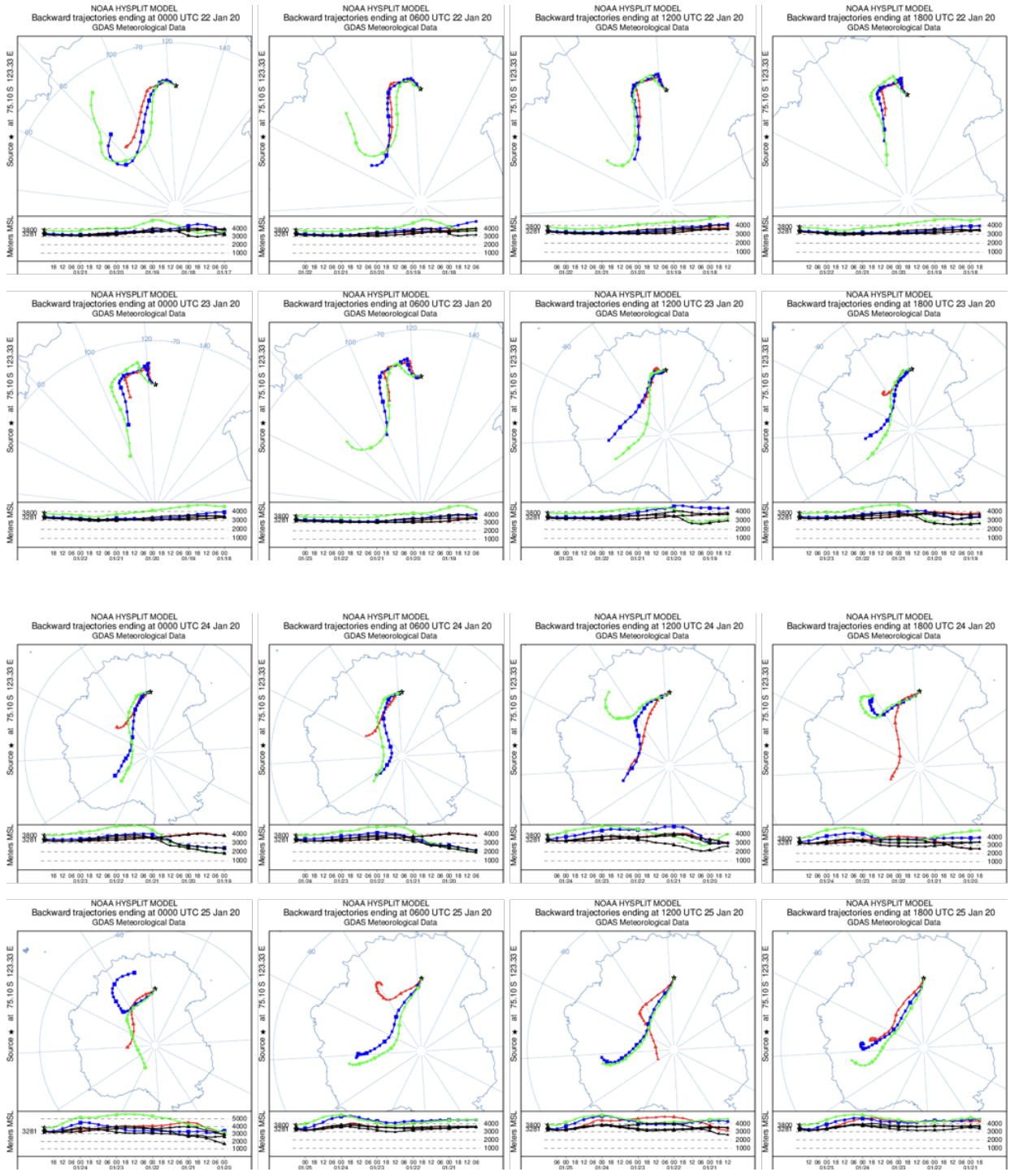

Figure A3. HYSPLIT 5 days backward trajectories from the 22^{nd} to the 25^{th} of January 2020. The model was run every 6 hours for each day and at 3 different altitudes: 3,800 a.m.s.l (green), 3,400 a.m.s.l (blue) and 3,200 a.m.s.l (red).

https://doi.org/10.5194/acp-2021-1018
Preprint. Discussion started: 15 December 2021
© Author(s) 2021. CC BY 4.0 License.

Atmospheric Chemistry and Physics Discussions

Figure A4 shows the HYSPLIT 10 days back trajectory estimation for the 23^{rd} of January ending at 20:00 LT at Dome C. One can see that for the 3,400 a.m.s.l, the model predicts air masses coming from the east coast of Antarctica, strengthening our conclusions of an air mass influenced by the ocean reaching the Antarctic Plateau, leading to the 10 ppbv O_3 drop observed in the early evening of the 23^{rd} of January 2020.

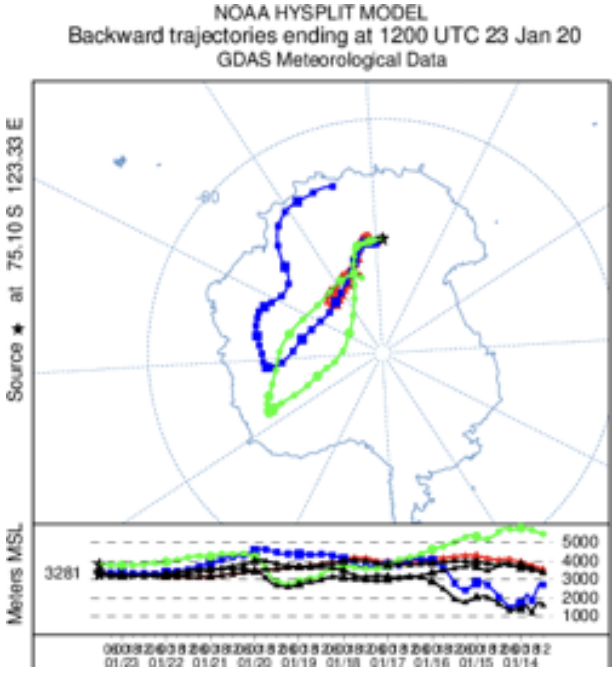

Figure A4. HYSPLIT 10 days backward trajectories of the 23^{rd} ending at 12:00 UTC (20:00 LT) at 3 different altitudes: 3,800 a.m.s.l (green), 3,400 a.m.s.l (blue) and 3,200 a.m.s.l (red).

https://doi.org/10.5194/acp-2021-1018
Preprint. Discussion started: 15 December 2021
© Author(s) 2021. CC BY 4.0 License.

Atmospheric Chemistry and Physics Discussions

Appendix B: Meteorological conditions during two periods of observations

The wind rose of the January period (Fig. B1d) shows strong wind from the West/North-West direction. Looking at Figure B1c, this event occurred in late January, around the 23^{rd}, strengthening our hypothesis of ocean air masses that might have reached Dome C at the end of January.

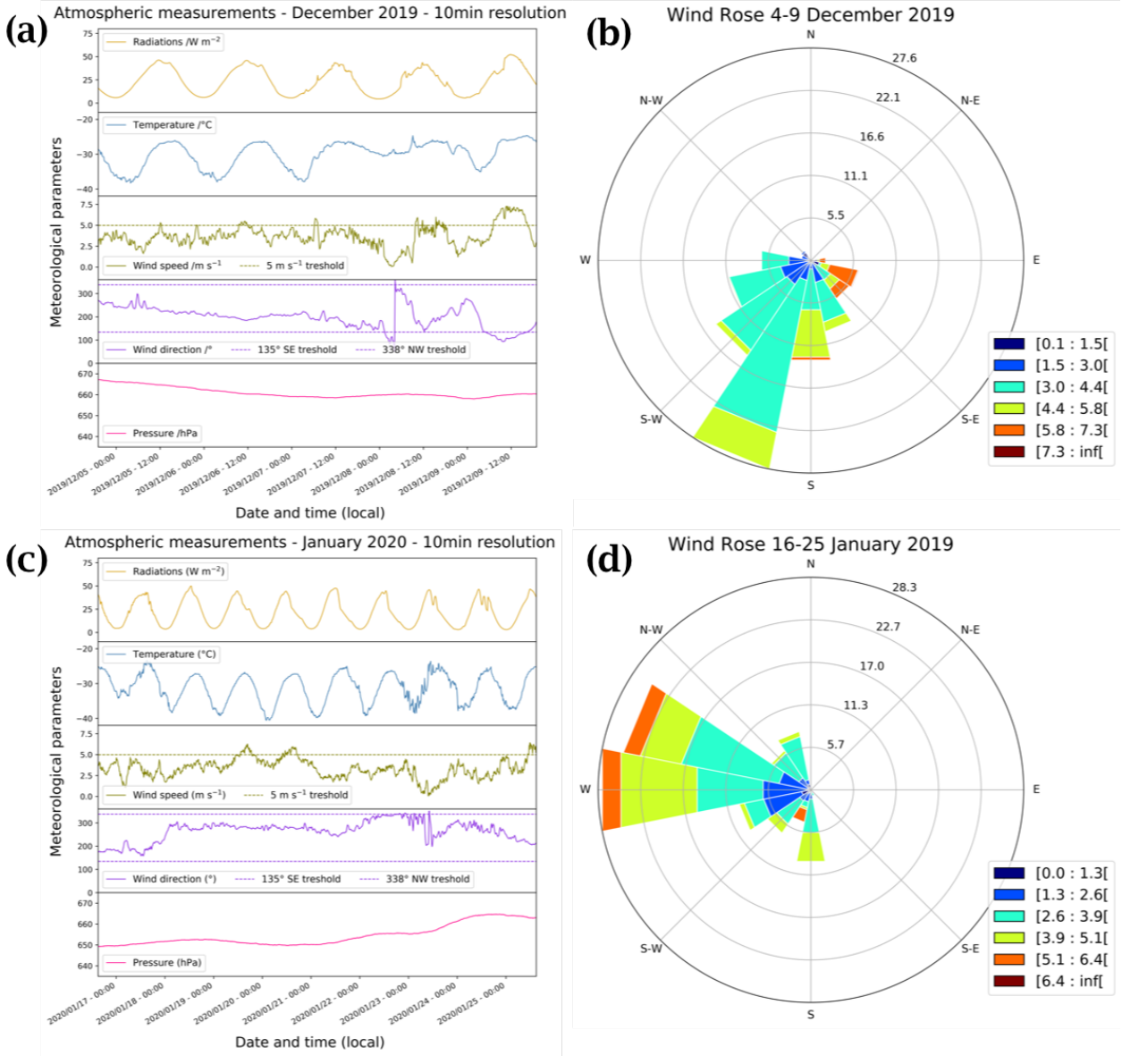

Figure B1. **(a)** and **(c)** Local meteorological conditions (2-m observations) encountered during the periods of atmospheric observations measured by the local automatic weather station (AWS– Vaisala Milos 520) completed with a broadband UV radiometer, spectral range 305–385 nm. **(b)** and **(d)** The corresponding wind rose in m s^{-1} at Dome C.

https://doi.org/10.5194/acp-2021-1018
Preprint. Discussion started: 15 December 2021
© Author(s) 2021. CC BY 4.0 License.

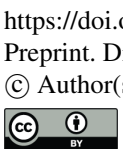

Atmospheric Chemistry and Physics Discussions

Appendix C: Snow-Tower experiment

Figure C1 shows the schematic of the snow-tower device, along with a photograph of one of the snow towers. We can see the two partially buried snow towers at the ends of the diagram, as well as the fully exposed atmospheric mast in the middle.

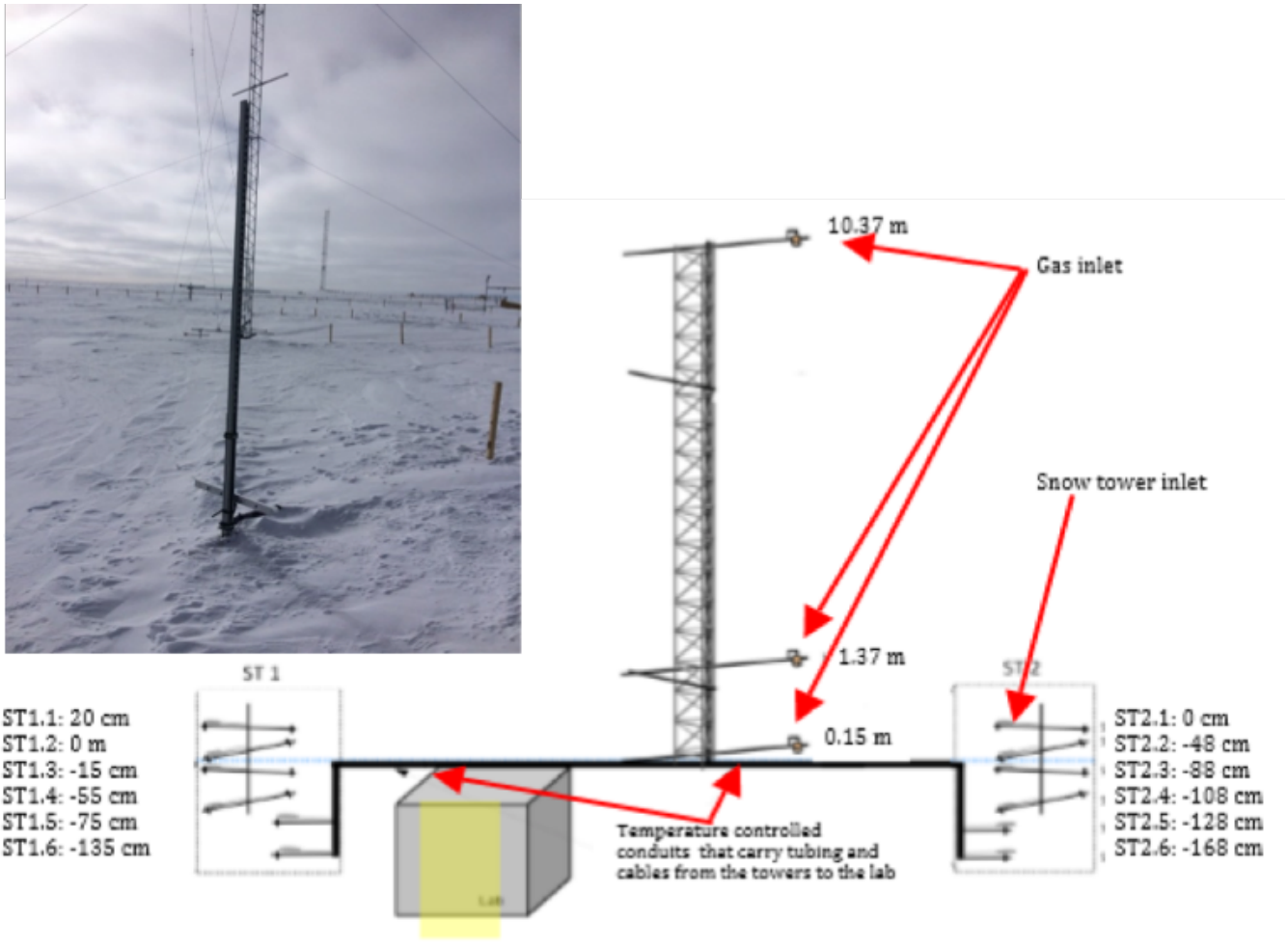

Figure C1. Snow-Tower installation at Dome C.

https://doi.org/10.5194/acp-2021-1018
Preprint. Discussion started: 15 December 2021
© Author(s) 2021. CC BY 4.0 License.

Atmospheric Chemistry and Physics Discussions

Appendix D: NO_2 and O^1D photolysis rate constant reconstruction: $J_{NO_{2-recons}}$ and $J_{O^1D_{-recons}}$

The $J_{NO_{2-recons}}$ [s^{-1}] is reconstructed using a correlation fit analysis between the UV radiations signal and the sparse J_{NO_2} measurements obtained with the MetCon 2π spectral radiometer (Fig. D1). A two degrees polynomial function, Equation D1, was found to be the best correlation fit (dashed black line in Fig. D1).

$$J_{NO_{2-recons}} = a + b \times UV + c \times UV^2 \quad \text{(D1)}$$

with $J_{NO_{2-recons}}$, the reconstructed photolysis rate coefficient; a, b and c, the regression fits parameters; and UV, the measured UV radiations.

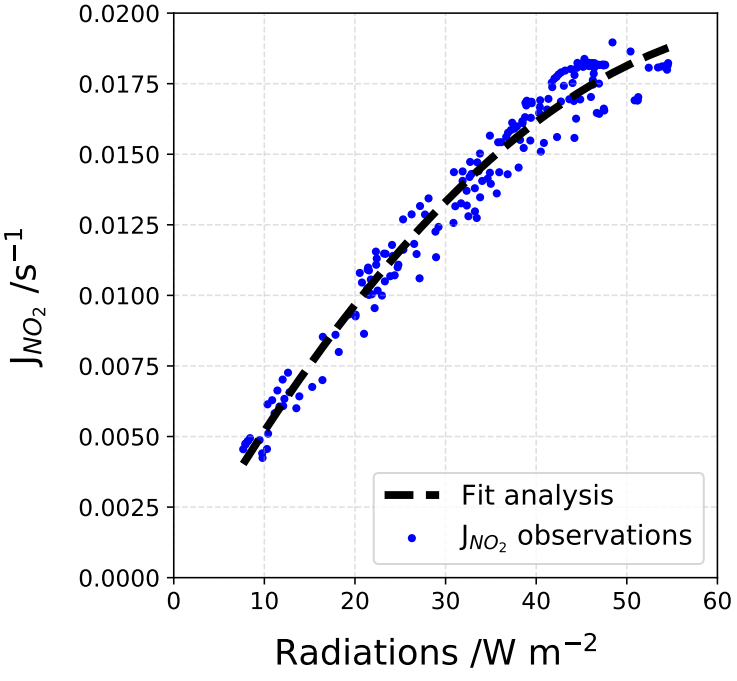

Figure D1. Fit analysis for the reconstruction of the J_{NO_2} signal.

Table D1 gives the values of a, b and c parameters for the photolysis rate constant at both periods.

Table D1. Polynomial regression fit parameters from Equation D1 applied to reconstruct the photolysis rate coefficient signal.

	$J_{NO_{2-recons}} = a + b \times UV + c \times UV^2$		
	a	b	c
December 4^{th} to 9^{th}	0.0	5.722×10^{-04}	-4.141×10^{-06}
January 16^{th} to 25^{th}	0.0	7.029×10^{-04}	-7.868×10^{-06}

https://doi.org/10.5194/acp-2021-1018
Preprint. Discussion started: 15 December 2021
© Author(s) 2021. CC BY 4.0 License.

Atmospheric Chemistry and Physics Discussions

Figure D2 represents the comparison between the reconstructed signal and the actual observations, on the bottom panel, the residual $\Delta J_{NO_{2-recons}}$ is represented showing a good agreement between the reconstructed signal and the original observations.

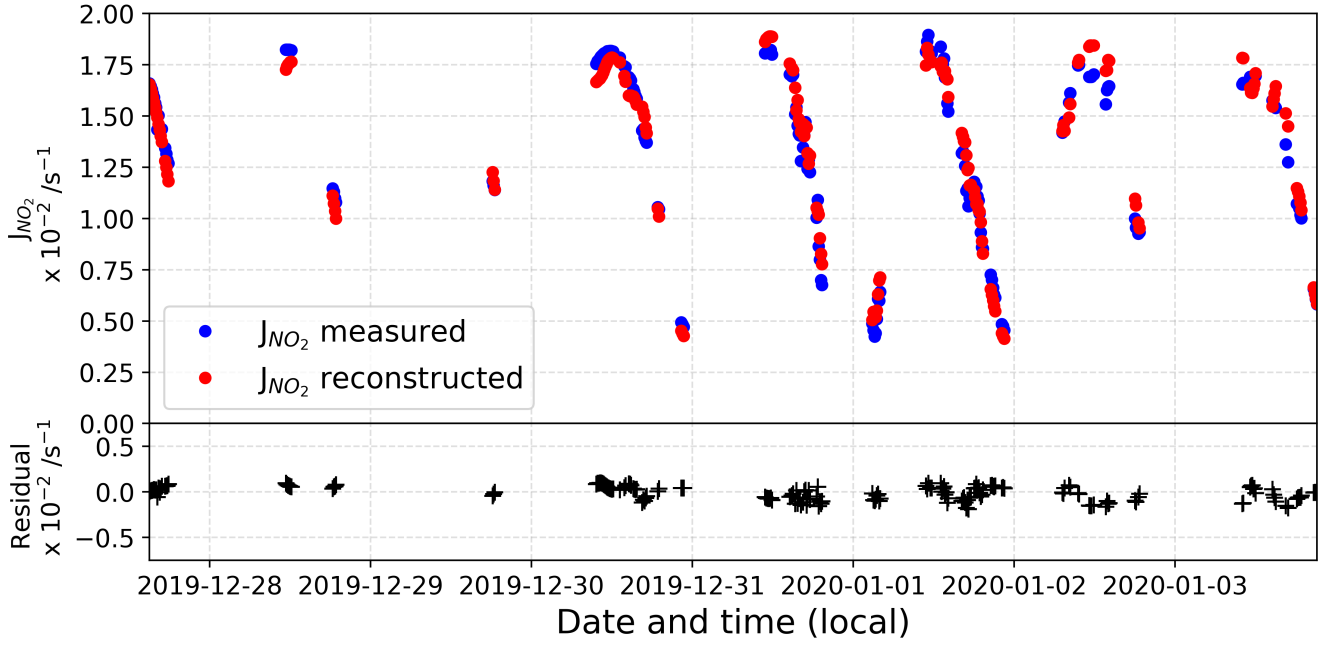

Figure D2. (top) Comparison between reconstructed and measured signal and **(bottom)** residual.

The $J_{O^1D_{-recons}}$ [s^{-1}] is reconstructed using a correlation fit analysis between the UV radiations signal and the sparse J_{O^1D} measurements obtained with the MetCon 2π spectral radiometer (Fig. D3). A two degrees polynomial function, Equation D2, was found to be the best correlation fit (dashed black line in Fig. D3).

$$J_{O^1D_{-recons}} = a + b \times UV + c \times UV^2 \quad \text{(D2)}$$

with $J_{O^1D_{-recons}}$, the reconstructed photolysis rate coefficient; a, b and c, the regression fits parameters; and UV, the measured UV radiations.

https://doi.org/10.5194/acp-2021-1018
Preprint. Discussion started: 15 December 2021
© Author(s) 2021. CC BY 4.0 License.

Atmospheric Chemistry and Physics Discussions

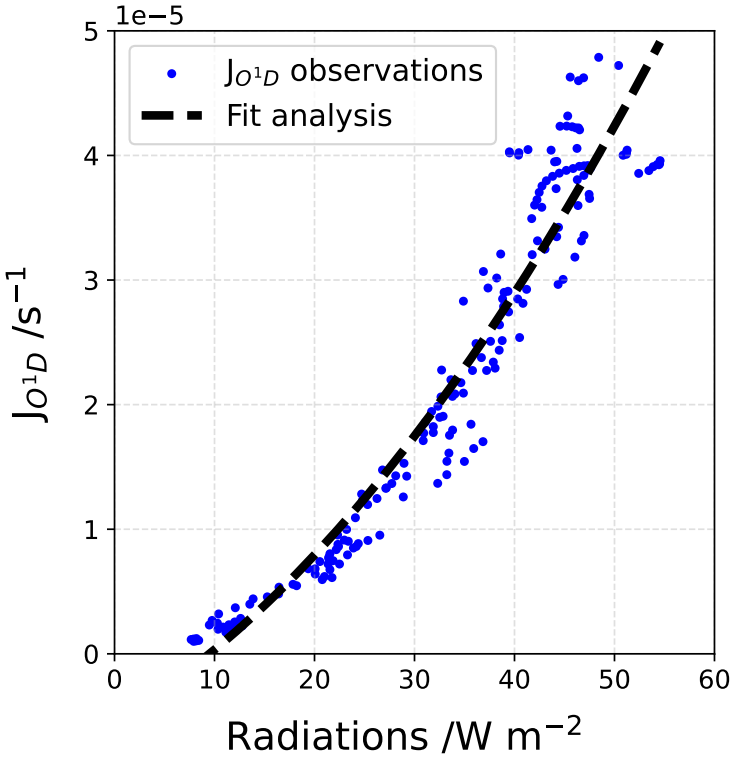

Figure D3. Fit analysis for the reconstruction of the $J_{O^1D_{-recons}}$ signal.

485 Table D2 gives the values of a, b and c parameters for the photolysis rate constant at both periods.

Table D2. Polynomial regression fit parameters from Equation D2 applied to reconstruct the photolysis rate coefficient signal.

	$J_{O^1D_{-recons}} = a + b \times UV + c \times UV^2$		
	a	b	c
December 4^{th} to 9^{th}	0.0	4.702×10^{-07}	9.674×10^{-09}
January 16^{th} to 25^{th}	0.0	6.251×10^{-07}	1.279×10^{-09}

Figure D4 represents the comparison between the reconstructed signal and the actual observations, on the bottom panel, the residual $\Delta J_{O^1D_{-recons}}$ is represented showing a good agreement between the reconstructed signal and the original observations.

https://doi.org/10.5194/acp-2021-1018
Preprint. Discussion started: 15 December 2021
© Author(s) 2021. CC BY 4.0 License.

Atmospheric Chemistry and Physics Discussions

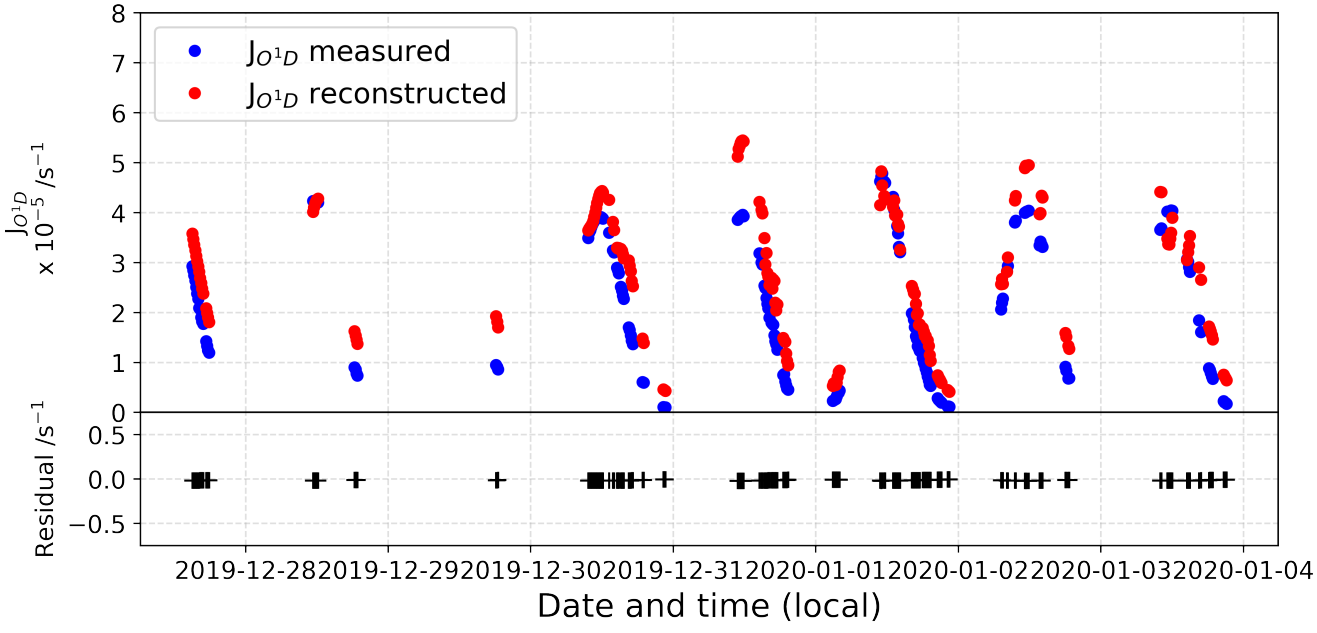

Figure D4. **(top)** Comparison between reconstructed and measured signal and **(bottom)** residual.

https://doi.org/10.5194/acp-2021-1018
Preprint. Discussion started: 15 December 2021
© Author(s) 2021. CC BY 4.0 License.

Atmospheric Chemistry and Physics Discussions

Appendix E: RO_x estimation from J_{NO_2}

Using the linear correlation between RO_2 and J_{NO_2} given by Kukui et al. (2014) (Fig. E1a); the RO_2 data from OPALE campaign (Kukui et al., 2014); and the reconstructed J_{NO_2} signal, we were able to estimate the RO_2 and HO_2 total number of molecules in the atmospheric boundary layer at Dome C during our periods of observation (Fig. E1b and E1c).

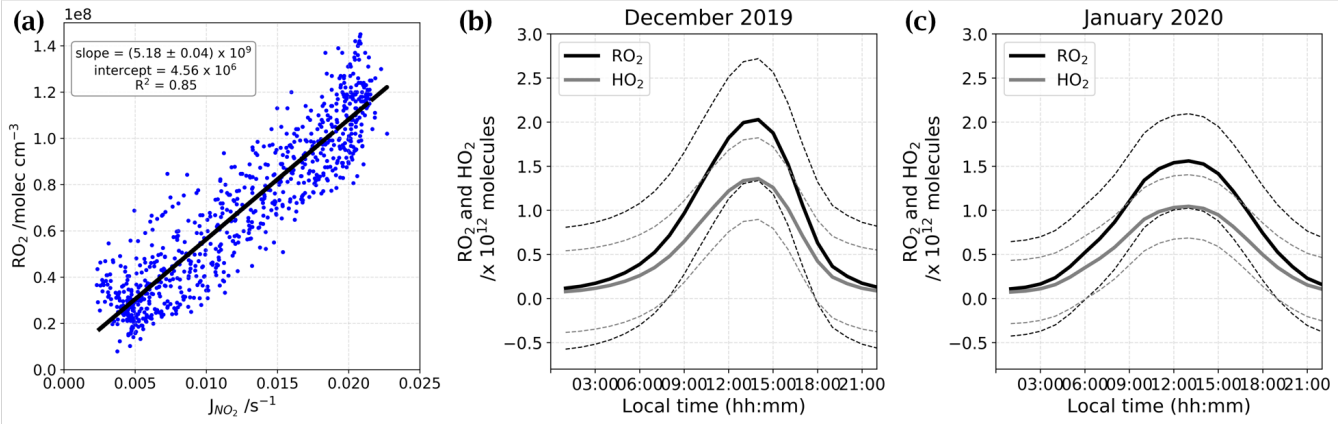

Figure E1. **(a)** linear correlation between RO_2 and J_{NO_2} taken from Kukui et al. (2014). **(b)** and **(c)** total number of molecules of RO_2 (black) and HO_2 (grey) estimated for both periods of observations residual.

https://doi.org/10.5194/acp-2021-1018
Preprint. Discussion started: 15 December 2021
© Author(s) 2021. CC BY 4.0 License.

Atmospheric Chemistry and Physics Discussions

Appendix F: Polar boundary layer height H_{PBL}

The regional climate model MAR, which has been applied extensively for studying the polar regions, e.g., Agosta et al. (2019); Gallée et al. (2015b); Gallée and Gorodetskaya (2010), was used in its latest Antarctic configuration: version 3.11 (Kittel et al., 2021), including drifting-snow physics (Amory et al., 2021) at 35 km resolution and forced by ERA5 reanalysis (https://www.ecmwf.int/en/forecasts) to generate the Boundary layer height extracted every hour to match the timestamp of our observations. Boundary layer height at Dome C during both periods of observations extracted from the regional model MAR are presented in Figure F1.

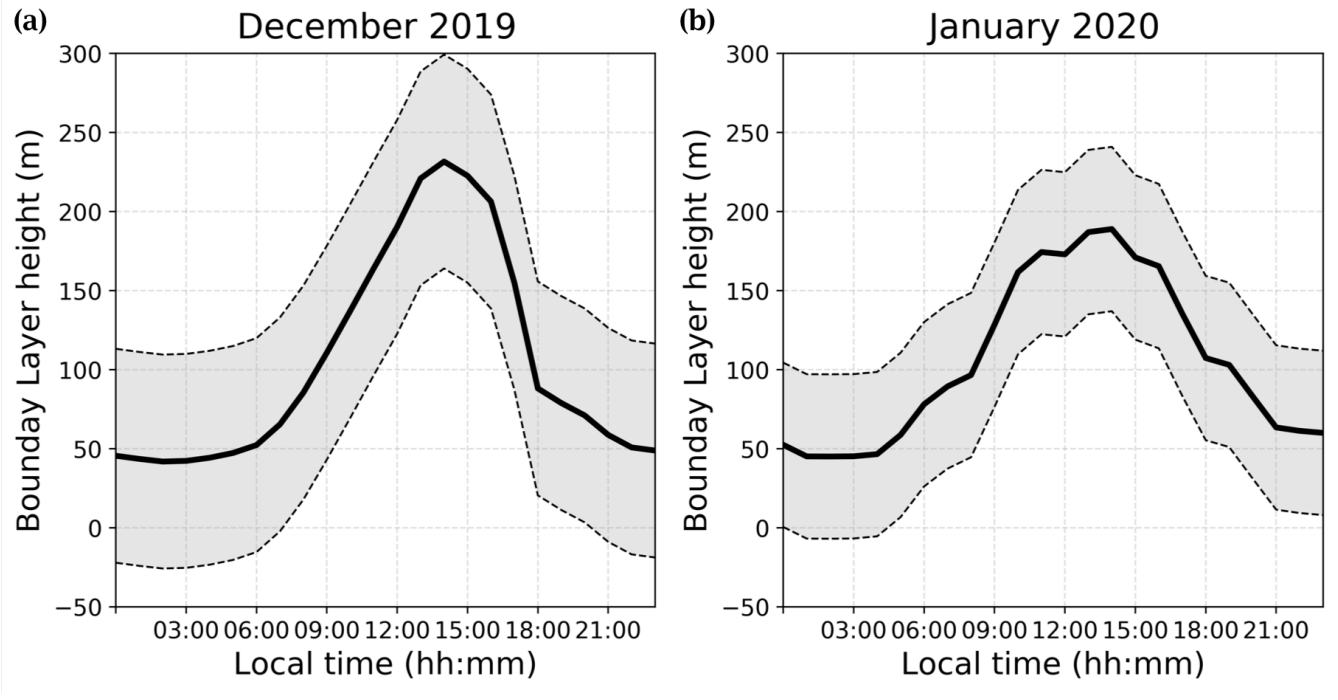

Figure F1. Atmospheric boundary layer height (PBL) (solid lines) $\pm$ 1σ (dashed lines) estimated for both periods by the MAR regional model.

https://doi.org/10.5194/acp-2021-1018
Preprint. Discussion started: 15 December 2021
© Author(s) 2021. CC BY 4.0 License.

Atmospheric Chemistry and Physics Discussions

Appendix G: Reactions and their chemical rates

The list of reactions at stakes in Dome C troposphere with the associated daily average chemical rates based on their expression given by Atkinson (1998, 2003); Atkinson et al. (2004, 2007), J_{NO_2} measurements and $J_{NO_3^-}$ estimation from Barbero et al. (2021), for Dome C conditions.

O_x reaction

$$O_3 + h\nu \rightarrow \text{products} \qquad (J_{O^1D} \approx 3.76 \times 10^{-5} s^{-1}) \tag{G1}$$

HO_x reaction

$$HO_2 + O_3 \rightarrow OH + 2O_2 \qquad (k_{HO_2+O_3} \approx 1.2 \times 10^{-15} cm^3 molecules^{-1} s^{-1}) \tag{G2}$$

NO_x reaction

$$OH + NO + M \rightarrow HONO + M \qquad (k_{OH+NO} \approx 1.0 \times 10^{-11} cm^3 molecules^{-1} s^{-1}) \tag{G3}$$

$$OH + NO_2 + M \rightarrow HONO_2 + M \qquad (k_{OH+NO_2} \approx 1.8 \times 10^{-11} cm^3 molecules^{-1} s^{-1}) \tag{G4}$$

$$HO_2 + NO \rightarrow OH + NO_2 \qquad (k_{HO_2+NO} \approx 1.1 \times 10^{-11} cm^3 molecules^{-1} s^{-1}) \tag{G5}$$

$$NO + O_3 \rightarrow NO_2 + O_2 \qquad (k_{NO+O_3} \approx 6.3 \times 10^{-15} cm^3 molecules^{-1} s^{-1}) \tag{G6}$$

$$HONO + h\nu \rightarrow \text{products} \qquad (J_{HONO} \approx 1.2 \times 10^{-3} s^{-1}) \tag{G7}$$

$$NO_2 + h\nu \rightarrow \text{products} \qquad (J_{NO_2} \approx 1.3 \times 10^{-2} s^{-1}) \tag{G8}$$

ClO_x reaction

$$ClO + NO \rightarrow Cl + NO_2 \qquad (k_{ClO+NO} \approx 2.1 \times 10^{-11} cm^3 molecules^{-1} s^{-1}) \tag{G9}$$

$$ClO + NO_2 + M \rightarrow ClONO_2 + M \qquad (k_{ClO+NO_2} \approx 2.0 \times 10^{-11} cm^3 molecules^{-1} s^{-1}) \tag{G10}$$

BrO_x reaction

$$BrO + NO \rightarrow Br + NO_2 \qquad (k_{BrO+NO} \approx 2.5 \times 10^{-11} cm^3 molecules^{-1} s^{-1}) \tag{G11}$$

$$BrO + NO_2 + M \rightarrow BrONO_2 + M \qquad (k_{BrO+NO_2} \approx 1.9 \times 10^{-11} cm^3 molecules^{-1} s^{-1}) \tag{G12}$$

IO_x reaction

$$IO + NO \rightarrow I + NO_2 \qquad (k_{IO+NO} \approx 2.8 \times 10^{-11} cm^3 molecules^{-1} s^{-1}) \tag{G13}$$

$$IO + NO_2 + M \rightarrow IONO_2 + M \qquad (k_{IO+NO_2} \approx 1.2 \times 10^{-11} cm^3 molecules^{-1} s^{-1}) \tag{G14}$$

From the list above, one can see that the chemical sources of NO_2 and sinks from RO_x and XO have similar rates.

https://doi.org/10.5194/acp-2021-1018
Preprint. Discussion started: 15 December 2021
© Author(s) 2021. CC BY 4.0 License.

Atmospheric Chemistry and Physics Discussions

Author contributions. Grants obtained by JS and RG funded the project. The IBBCEAS instruments were designed, developed and validated by CB and AB under the supervision of RG. JS, RG, NC, MMF and DH contributed with their knowledge in atmospheric sciences. NC provided technical and engineering support during the 2019-2020 Antarctic campaign. The paper was written by AB, with contributions from all authors.

Data availability. The data used in this study "will be available at PDI-30390: Data submission 2021-12-07T09:55:41Z" with license "CC-BY: Creative Commons Attribution 4.0 International".

Competing interests. The authors declare that they have no conflict of interest.

Acknowledgements. The research leading to these results has received funding from: the LabEx OSUG@2020 ("Investissements d'avenir" – ANR10 LABX56) ; the French National program LEFE (Les Enveloppes Fluides et l'Environnement) via LEFE REACT ; the Agence Nationale de la Recherche (ANR) via contract ANR-16-CE01-0011-01 EAIIST ; the Foundation BNP-Paribas through its Climate & Biodiversity Initiative program and by the French Polar Institute (IPEV) through programs 1177 (CAPOXI 35–75) and 1169 (EAIIST). The meteorological data and information were obtained from IPEV/PNRA Project "Routine Meteorological Observation at Station Concordia" http://www.climantartide.it. The data used in this publication for the irradiations fluxes were obtained from LATMOS, with the help of Florence Goutail et Jean-Pierre Pommereau as part of the Network for the Detection of Atmospheric Composition Change (NDACC) and are publicly available (see http://www.ndacc.org). The authors thank Holly Winton for her help with the MetCon data processing. The authors gratefully acknowledge the NOAA Air Resources Laboratory (ARL) for the provision of the HYSPLIT transport and dispersion model and READY website (https://www.ready.noaa.gov) used in this publication. The authors thanks Charles Amory for running the MAR regional model and providing the PBL height. We greatly thank Holly Winton for her help with the MetCon data retrieving and analysis. The authors particularly thank Pete Akers for his help with the English edits of the manuscript. Detlev Helming's contributions and the installation and operation of the snow tower platform were supported through a grant from the National Science Foundation (NSF), PLR#1142145. Markus M. Frey is supported by core funding from UK NERC to BAS's Atmosphere, Ice and Climate program. Finally, the authors greatly thank the technical staff of the IGE and IPEV for their technical and logistic support in Grenoble and during the field campaign.

https://doi.org/10.5194/acp-2021-1018
Preprint. Discussion started: 15 December 2021
© Author(s) 2021. CC BY 4.0 License.

Atmospheric Chemistry and Physics Discussions

References

Agosta, C., Amory, C., Kittel, C., Orsi, A., Favier, V., Gallée, H., van den Broeke, M. R., Lenaerts, J. T. M., van Wessem, J. M., van de Berg, W. J., and Fettweis, X.: Estimation of the Antarctic surface mass balance using the regional climate model MAR (1979–2015) and identification of dominant processes, The Cryosphere, 13, 281–296, https://doi.org/10.5194/tc-13-281-2019, 2019.

Amory, C., Kittel, C., Le Toumelin, L., Agosta, C., Delhasse, A., Favier, V., and Fettweis, X.: Performance of MAR (v3.11) in simulating the drifting-snow climate and surface mass balance of Adélie Land, East Antarctica, Geoscientific Model Development, 14, 3487–3510, https://doi.org/10.5194/gmd-14-3487-2021, 2021.

Anderson, P. S. and Bauguitte, S. J.-B.: Behaviour of tracer diffusion in simple atmospheric boundary layer models, Atmospheric Chemistry and Physics, 7, 5147–5158, https://doi.org/10.5194/acp-7-5147-2007, 2007.

Atkinson, D. B.: Solving chemical problems of environmental importance using Cavity Ring-Down Spectroscopy, The Analyst, 128, 117–125, https://doi.org/10.1039/b206699h, 2003.

Atkinson, R.: Atmospheric chemistry of VOCs and NOV, Atmospheric Environment, 34, 2063–2101, https://doi.org/10.1016/S1352-2310(99)00460-4, 1998.

Atkinson, R., Baulch, D. L., Cox, R. A., Crowley, J. N., Hampson, R. F., Hynes, R. G., Jenkin, M. E., Rossi, M. J., and Troe, J.: Evaluated kinetic and photochemical data for atmospheric chemistry: Volume I - gas phase reactions of O_x, HO_x, NO_x and SO_x species, Atmospheric Chemistry and Physics, 4, 1461–1738, https://doi.org/10.5194/acp-4-1461-2004, 2004.

Atkinson, R., Baulch, D. L., Cox, R. A., Crowley, J. N., Hampson, R. F., Hynes, R. G., Jenkin, M. E., Rossi, M. J., and Troe, J.: Evaluated kinetic and photochemical data for atmospheric chemistry: Volume III – gas phase reactions of inorganic halogens, Atmospheric Chemistry and Physics, 7, 981–1191, https://doi.org/10.5194/acp-7-981-2007, 2007.

Barbero, A., Blouzon, C., Savarino, J., Caillon, N., Dommergue, A., and Grilli, R.: A compact incoherent broadband cavity-enhanced absorption spectrometer for trace detection of nitrogen oxides, iodine oxide and glyoxal at levels below parts per billion for field applications, Atmospheric Measurement Techniques, 13, 4317–4331, https://doi.org/10.5194/amt-13-4317-2020, 2020.

Barbero, A., Savarino, J., Grilli, R., Blouzon, C., Picard, G., Frey, M. M., Huang, Y., and Caillon, N.: New Estimation of the NO_x Snow-Source on the Antarctic Plateau, Journal of Geophysical Research: Atmospheres, 126, https://doi.org/10.1029/2021JD035062, 2021.

Bauguitte, S. J.-B., Bloss, W. J., Evans, M. J., Salmon, R. A., Anderson, P. S., Jones, A. E., Lee, J. D., Saiz-Lopez, A., Roscoe, H. K., Wolff, E. W., and Plane, J. M. C.: Summertime NO_x measurements during the CHABLIS campaign: can source and sink estimates unravel observed diurnal cycles?, Atmospheric Chemistry and Physics, 12, 989–1002, https://doi.org/10.5194/acp-12-989-2012, 2012.

Beine, H. J., Honrath, R. E., Dominé, F., Simpson, W. R., and Fuentes, J. D.: NO_x during background and ozone depletion periods at Alert: Fluxes above the snow surface, Journal of Geophysical Research, 107, 12, https://doi.org/10.1029/2002JD002082, 2002.

Berhanu, T. A., Savarino, J., Erbland, J., Vicars, W. C., Preunkert, S., Martins, J. F., and Johnson, M. S.: Isotopic effects of nitrate photochemistry in snow: a field study at Dome C, Antarctica, Atmospheric Chemistry and Physics, 15, 11 243–11 256, https://doi.org/10.5194/acp-15-11243-2015, 2015.

Berresheim, H. and Eisele, F. L.: Sulfur Chemistry in the Antarctic Troposphere Experiment: An overview of project SCATE, Journal of Geophysical Research: Atmospheres, 103, 1619–1627, https://doi.org/10.1029/97JD00103, 1998.

Bloss, W. J., Lee, J. D., Heard, D. E., and Salmon, R. A.: Observations of OH and HO_2 radicals in coastal Antarctica, Atmospheric Chemistry and Physics, 7, 4171–4185, https://doi.org/10.5194/acp-7-4171-2007, 2007.

https://doi.org/10.5194/acp-2021-1018
Preprint. Discussion started: 15 December 2021
© Author(s) 2021. CC BY 4.0 License.

Bloss, W. J., Camredon, M., Lee, J. D., Heard, D. E., Plane, J. M. C., Saiz-Lopez, A., Bauguitte, S. J.-B., Salmon, R. A., and Jones, A. E.: Coupling of HO_x, NO_x and halogen chemistry in the Antarctic boundary layer, Atmospheric Chemistry and Physics, 10, 10 187–10 209, https://doi.org/10.5194/acp-10-10187-2010, 2010.

Bock, J., Savarino, J., and Picard, G.: Air–snow exchange of nitrate: a modelling approach to investigate physicochemical processes in surface snow at Dome C, Antarctica, Atmospheric Chemistry and Physics, 16, 12 531–12 550, https://doi.org/10.5194/acp-16-12531-2016, 2016.

Davis, D., Nowak, J. B., Chen, G., Buhr, M., Arimoto, R., Hogan, A., Eisele, F., Mauldin, L., Tanner, D., Shetter, R., Lefer, B., and McMurry, P.: Unexpected high levels of NO observed at South Pole, Geophysical Research Letters, 28, 3625–3628, https://doi.org/10.1029/2000GL012584, 2001.

Davis, D., Eisele, F., Chen, G., Crawford, J., Huey, G., Tanner, D., Slusher, D., Mauldin, L., Oncley, S., Lenschow, D., Semmer, S., Shetter, R., Lefer, B., Arimoto, R., Hogan, A., Grube, P., Lazzara, M., Bandy, A., Thornton, D., Berresheim, H., Bingemer, H., Hutterli, M., McConnell, J., Bales, R., Dibb, J., Buhr, M., Park, J., McMurry, P., Swanson, A., Meinardi, S., and Blake, D.: An overview of ISCAT 2000, Atmospheric Environment, 38, 5363–5373, https://doi.org/10.1016/j.atmosenv.2004.05.037, 2004.

Davis, D., Seelig, J., Huey, G., Crawford, J., Chen, G., Wang, Y., Buhr, M., Helmig, D., Neff, W., and Blake, D.: A reassessment of Antarctic plateau reactive nitrogen based on ANTCI 2003 airborne and ground based measurements, Atmospheric Environment, 42, 2831–2848, https://doi.org/10.1016/j.atmosenv.2007.07.039, 2008.

Eisele, F., Davis, D., Helmig, D., Oltmans, S., Neff, W., Huey, G., Tanner, D., Chen, G., Crawford, J., and Arimoto, R.: Antarctic Tropospheric Chemistry Investigation (ANTCI) 2003 overview, Atmospheric Environment, 42, 2749–2761, https://doi.org/10.1016/j.atmosenv.2007.04.013, 2008.

EPICA community members: Eight glacial cycles from an Antarctic ice core, Nature, 429, 623–628, https://doi.org/10.1038/nature02599, 2004.

Erbland, J., Vicars, W. C., Savarino, J., Morin, S., Frey, M. M., Frosini, D., Vince, E., and Martins, J. M. F.: Air–snow transfer of nitrate on the East Antarctic Plateau – Part 1: Isotopic evidence for a photolytically driven dynamic equilibrium in summer, Atmospheric Chemistry and Physics, 13, 6403–6419, https://doi.org/10.5194/acp-13-6403-2013, 2013.

Erbland, J., Savarino, J., Morin, S., France, J. L., Frey, M. M., and King, M. D.: Air–snow transfer of nitrate on the East Antarctic Plateau – Part 2: An isotopic model for the interpretation of deep ice-core records, Atmospheric Chemistry and Physics, 15, 12 079–12 113, https://doi.org/10.5194/acp-15-12079-2015, 2015.

Frey, M. M.: Frey, M.M., Atmospheric NO_x mixing ratios at Dome C (East Antarctica) during the OPALE campaign in austral summer 2011/12', Polar Data Centre, Natural Environment Research Council, UK Research & Innovation,, https://doi.org/submitted 2021, 2021.

Frey, M. M., Savarino, J., Morin, S., Erbland, J., and Martins, J. M. F.: Photolysis imprint in the nitrate stable isotope signal in snow and atmosphere of East Antarctica and implications for reactive nitrogen cycling, Atmospheric Chemistry and Physics, 9, 8681–8696, https://doi.org/10.5194/acp-9-8681-2009, 2009.

Frey, M. M., Brough, N., France, J. L., Anderson, P. S., Traulle, O., King, M. D., Jones, A. E., Wolff, E. W., and Savarino, J.: The diurnal variability of atmospheric nitrogen oxides (NO and NO_2) above the antarctic plateau driven by atmospheric stability and snow emissions, Atmospheric Chemistry and Physics, 13, 3045–3062, https://doi.org/10.5194/acp-13-3045-2013, 2013.

Frey, M. M., Roscoe, H. K., Kukui, A., Savarino, J., France, J. L., King, M. D., Legrand, M., and Preunkert, S.: Atmospheric nitrogen oxides (NO and NO_2) at Dome C, East Antarctica, during the OPALE campaign, Atmospheric Chemistry and Physics, 15, 7859–7875, https://doi.org/10.5194/acp-15-7859-2015, 2015.

https://doi.org/10.5194/acp-2021-1018
Preprint. Discussion started: 15 December 2021
© Author(s) 2021. CC BY 4.0 License.

Atmospheric Chemistry and Physics Discussions

Gallée, H. and Gorodetskaya, I. V.: Validation of a limited area model over Dome C, Antarctic Plateau, during winter, Climate Dynamics, 34, 61–72, https://doi.org/10.1007/s00382-008-0499-y, 2010.

Gallée, H., Barral, H., Vignon, E., and Genthon, C.: A case study of a low-level jet during OPALE, Atmospheric Chemistry and Physics, 15, 6237–6246, https://doi.org/10.5194/acp-15-6237-2015, 2015a.

Gallée, H., Preunkert, S., Argentini, S., Frey, M. M., Genthon, C., Jourdain, B., Pietroni, I., Casasanta, G., Barral, H., Vignon, E., Amory, C., and Legrand, M.: Characterization of the boundary layer at Dome C (East Antarctica) during the OPALE summer campaign, Atmospheric Chemistry and Physics, 15, 6225–6236, https://doi.org/10.5194/acp-15-6225-2015, 2015b.

Genthon, C., Town, M. S., Six, D., Favier, V., Argentini, S., and Pellegrini, A.: Meteorological atmospheric boundary layer measurements and ECMWF analyses during summer at Dome C, Antarctica, Journal of Geophysical Research, 115, D05 104, https://doi.org/10.1029/2009JD012741, 2010.

Grannas, A. M., Jones, A. E., Dibb, J., Ammann, M., Anastasio, C., Beine, H. J., Bergin, M., Bottenheim, J., Boxe, C. S., Carver, G., Chen, G., Crawford, J. H., Domine, F., Frey, M. M., Guzman, M. I., Heard, D. E., Helmig, D., Hoffmann, M. R., Honrath, R. E., Huey, L. G., Hutterli, M., Jacobi, H. W., Klan, P., Lefer, B., McConnell, J., Plane, J., Sander, R., Savarino, J., Shepson, P. B., Simpson, W. R., Sodeau, J. R., Weller, R., Wolff, E. W., and Zhu, T.: An overview of snow photochemistry: evidence, mechanisms and impacts, Atmospheric Chemistry and Physics, 7, 4329–4373, https://doi.org/10.5194/acp-7-4329-2007, 2007.

Helmig, D., Johnson, B., Warshawsky, M., Morse, T., Neff, W., Eisele, F., and Davis, D.: Nitric oxide in the boundary-layer at South Pole during the Antarctic Tropospheric Chemistry Investigation (ANTCI), Atmospheric Environment, 42, 2817–2830, https://doi.org/10.1016/j.atmosenv.2007.03.061, 2008.

Helmig, D., Liptzin, D., Hueber, J., and Savarino, J.: Impact of exhaust emissions on chemical snowpack composition at Concordia Station, Antarctica, The Cryosphere, 14, 199–209, https://doi.org/10.5194/tc-14-199-2020, 2020.

Jones, A. E., Wolff, E. W., Salmon, R. A., Clemitshaw, K. C., Fleming, Z. L., Bloss, W. J., Heard, D. E., Lee, J. D., Read, K. A., Hamer, P., Shallcross, D. E., Jackson, A. V., Walker, S. L., Lewis, A. C., Mills, G. P., Plane, J. M. C., Saiz-Lopez, A., Sturges, W. T., and Worton, D. R.: Chemistry of the Antarctic Boundary Layer and the Interface with Snow: an overview of the CHABLIS campaign, Atmospheric Chemistry and Physics, 8, 3789–3803, https://doi.org/https://doi.org/10.5194/acp-8-3789-2008, 2008.

Jones, A. E., Wolff, E. W., Ames, D., Bauguitte, S. J.-B., Clemitshaw, K. C., Fleming, Z., Mills, G. P., Saiz-Lopez, A., Salmon, R. A., Sturges, W. T., and Worton, D. R.: The multi-seasonal NO_y budget in coastal Antarctica and its link with surface snow and ice core nitrate: results from the CHABLIS campaign, Atmospheric Chemistry and Physics, 11, 9271–9285, https://doi.org/10.5194/acp-11-9271-2011, 2011.

Kittel, C., Amory, C., Agosta, C., Jourdain, N. C., Hofer, S., Delhasse, A., Doutreloup, S., Huot, P.-V., Lang, C., Fichefet, T., and Fettweis, X.: Diverging future surface mass balance between the Antarctic ice shelves and grounded ice sheet, The Cryosphere, 15, 1215–1236, https://doi.org/10.5194/tc-15-1215-2021, 2021.

Kukui, A., Legrand, M., Preunkert, S., Frey, M. M., Loisil, R., Gil Roca, J., Jourdain, B., King, M. D., France, J. L., and Ancellet, G.: Measurements of OH and RO_2 radicals at Dome C, East Antarctica, Atmospheric Chemistry and Physics, 14, 12 373–12 392, https://doi.org/10.5194/acp-14-12373-2014, 2014.

Kuttippurath, J., Goutail, F., Pommereau, J.-P., Lefèvre, F., Roscoe, H. K., Pazmiño, A., Feng, W., Chipperfield, M. P., and Godin-Beekmann, S.: Estimation of Antarctic ozone loss from ground-based total column measurements, Atmospheric Chemistry and Physics, 10, 6569–6581, https://doi.org/10.5194/acp-10-6569-2010, 2010.

https://doi.org/10.5194/acp-2021-1018
Preprint. Discussion started: 15 December 2021
© Author(s) 2021. CC BY 4.0 License.

Legrand, M., Preunkert, S., Jourdain, B., Gallée, H., Goutail, F., Weller, R., and Savarino, J.: Year-round record of surface ozone at coastal (Dumont d'Urville) and inland (Concordia) sites in East Antarctica, Journal of Geophysical Research, 114, D20 306, https://doi.org/10.1029/2008JD011667, 2009.

Legrand, M., Preunkert, S., Frey, M., Bartels-Rausch, T., Kukui, A., King, M. D., Savarino, J., Kerbrat, M., and Jourdain, B.: Large mixing ratios of atmospheric nitrous acid (HONO) at Concordia (East Antarctic Plateau) in summer: a strong source from surface snow?, Atmospheric Chemistry and Physics, 14, 9963–9976, https://doi.org/10.5194/acp-14-9963-2014, 2014.

Legrand, M., Preunkert, S., Savarino, J., Frey, M. M., Kukui, A., Helmig, D., Jourdain, B., Jones, A. E., Weller, R., Brough, N., and Gallée, H.: Inter-annual variability of surface ozone at coastal (Dumont d'Urville, 2004–2014) and inland (Concordia, 2007–2014) sites in East Antarctica, Atmospheric Chemistry and Physics, 16, 8053–8069, https://doi.org/10.5194/acp-16-8053-2016, 2016.

Leighton, P. A.: Photochemistry of Air Pollution, Academic Press, New York, 1961.

Libois, Q., Picard, G., France, J. L., Arnaud, L., Dumont, M., Carmagnola, C. M., and King, M. D.: Influence of grain shape on light penetration in snow, The Cryosphere, 7, 1803–1818, https://doi.org/10.5194/tc-7-1803-2013, 2013.

Libois, Q., Picard, G., Dumont, M., Arnaud, L., Sergent, C., Pougatch, E., Sudul, M., and Vial, D.: Experimental determination of the absorption enhancement parameter of snow, Journal of Glaciology, 60, 714–724, https://doi.org/10.3189/2014JoG14J015, 2014.

Mauldin, R. L., Eisele, F. L., Tanner, D. J., Kosciuch, E., Shetter, R., Lefer, B., Hall, S. R., Nowak, J. B., Buhr, M., Chen, G., Wang, P., and Davis, D.: Measurements of OH, H_2SO_4 and MSA at the South Pole during ISCAT, Geophysical Research Letters, 28, 3629–3632, https://doi.org/10.1029/2000GL012711, 2001.

Meusinger, C., Berhanu, T. A., Erbland, J., Savarino, J., and Johnson, M. S.: Laboratory study of nitrate photolysis in Antarctic snow. I. Observed quantum yield, domain of photolysis, and secondary chemistry, The Journal of Chemical Physics, 140, 244 305, https://doi.org/10.1063/1.4882898, 2014.

Mills, G. P., Sturges, W. T., Salmon, R. A., Bauguitte, S. J.-B., Read, K. A., and Bandy, B. J.: Seasonal variation of peroxyacetylnitrate (PAN) in coastal Antarctica measured with a new instrument for the detection of sub-part per trillion mixing ratios of PAN, Atmospheric Chemistry and Physics, 7, 4589–4599, https://doi.org/10.5194/acp-7-4589-2007, 2007.

Pommereau, J. P. and Goutail, F.: Stratospheric O_3 and NO_2 observations at the southern polar circle in summer and fall 1988, Geophysical Research Letters, 15, 895–897, https://doi.org/10.1029/GL015i008p00895, 1988.

Preunkert, S., Ancellet, G., Legrand, M., Kukui, A., Kerbrat, M., Sarda-Estève, R., Gros, V., and Jourdain, B.: Oxidant Production over Antarctic Land and its Export (OPALE) project: an overview of the 2010-2011 summer campaign: overview of the OPALE project 2010-2011, Journal of Geophysical Research: Atmospheres, 117, 307–319, https://doi.org/10.1029/2011JD017145, 2012.

Preunkert, S., Legrand, M., Frey, M. M., Kukui, A., Savarino, J., Gallée, H., King, M., Jourdain, B., Vicars, W., and Helmig, D.: Formaldehyde (HCHO) in air, snow, and interstitial air at Concordia (East Antarctic Plateau) in summer, Atmospheric Chemistry and Physics, 15, 6689–6705, https://doi.org/10.5194/acp-15-6689-2015, 2015.

Read, K. A., Lewis, A. C., Bauguitte, S., Rankin, A. M., Salmon, R. A., Wolff, E. W., Saiz-Lopez, A., Bloss, W. J., Heard, D. E., Lee, J. D., and Plane, J. M. C.: DMS and MSA measurements in the Antarctic Boundary Layer: impact of BrO on MSA production, Atmospheric Chemistry and Physics, 8, 2985–2997, https://doi.org/10.5194/acp-8-2985-2008, 2008.

Reed, C., Evans, M. J., Di Carlo, P., Lee, J. D., and Carpenter, L. J.: Interferences in photolytic NO_2 measurements: explanation for an apparent missing oxidant?, Atmospheric Chemistry and Physics, 16, 4707–4724, https://doi.org/10.5194/acp-16-4707-2016, 2016.

https://doi.org/10.5194/acp-2021-1018
Preprint. Discussion started: 15 December 2021
© Author(s) 2021. CC BY 4.0 License.

Ridley, B., Walega, J., Montzka, D., Grahek, F., Atlas, E., Flocke, F., Stroud, V., Deary, J., Gallant, A., Boudries, H., Bottenheim, J., Anlauf, K., Worthy, D., Sumner, A. L., Splawn, B., and Shepson, P.: Is the Arctic surface layer a source and sink of NO_x in Winter/Spring?, Journal of Atmospheric Chemistry, 36, 1–22, https://doi.org/10.1023/A:1006301029874, 2000.

Rolph, G., Stein, A., and Stunder, B.: Real-time Environmental Applications and Display sYstem: READY, Environmental Modelling & Software, 95, 210–228, https://doi.org/10.1016/j.envsoft.2017.06.025, 2017.

Roscoe, H., Brough, N., Jones, A., Wittrock, F., Richter, A., Van Roozendael, M., and Hendrick, F.: Characterisation of vertical BrO distribution during events of enhanced tropospheric BrO in Antarctica, from combined remote and in-situ measurements, Journal of Quantitative Spectroscopy and Radiative Transfer, 138, 70–81, https://doi.org/10.1016/j.jqsrt.2014.01.026, 2014.

Saiz-Lopez, A., Plane, J. M. C., Mahajan, A. S., Anderson, P. S., Bauguitte, S. J.-B., Jones, A. E., Roscoe, H. K., Salmon, R. A., Bloss, W. J., Lee, J. D., and Heard, D. E.: On the vertical distribution of boundary layer halogens over coastal Antarctica: implications for O_3, HO_x, NO_x and the Hg lifetime, Atmospheric Chemistry and Physics, 8, 887–900, https://doi.org/10.5194/acp-8-887-2008, 2008.

Salmon, R. A., Bauguitte, S. J.-B., Bloss, W., Hutterli, M. A., Jones, A. E., Read, K., and Wolff, E. W.: Measurement and interpretation of gas phase formaldehyde concentrations obtained during the CHABLIS campaign in coastal Antarctica, Atmospheric Chemistry and Physics, 8, 4085–4093, https://doi.org/10.5194/acp-8-4085-2008, 2008.

Savarino, J., Kaiser, J., Morin, S., Sigman, D. M., and Thiemens, M. H.: Nitrogen and oxygen isotopic constraints on the origin of atmospheric nitrate in coastal Antarctica, Atmospheric Chemistry and Physics, 7, 1925–1945, https://doi.org/10.5194/acp-7-1925-2007, 2007.

Savarino, J., Vicars, W. C., Legrand, M., Preunkert, S., Jourdain, B., Frey, M. M., Kukui, A., Caillon, N., and Roca, J. G.: Oxygen isotope mass balance of atmospheric nitrate at Dome C, East Antarctica, during the OPALE campaign, Atmospheric Chemistry and Physics, 16, 2659–2673, https://doi.org/10.5194/acp-16-2659-2016, 2016.

Schönhardt, A., Richter, A., Wittrock, F., Kirk, H., Oetjen, H., Roscoe, H. K., and Burrows, J. P.: Observations of iodine monoxide columns from satellite, Atmospheric Chemistry and Physics, 8, 637–653, https://doi.org/10.5194/acp-8-637-2008, 2008.

Schönhardt, A., Begoin, M., Richter, A., Wittrock, F., Kaleschke, L., Gómez Martín, J. C., and Burrows, J. P.: Simultaneous satellite observations of IO and BrO over Antarctica, Atmospheric Chemistry and Physics, 12, 6565–6580, https://doi.org/10.5194/acp-12-6565-2012, 2012.

Spolaor, A., Burgay, F., Fernandez, R. P., Turetta, C., Cuevas, C. A., Kim, K., Kinnison, D. E., Lamarque, J.-F., de Blasi, F., Barbaro, E., Corella, J. P., Vallelonga, P., Frezzotti, M., Barbante, C., and Saiz-Lopez, A.: Antarctic ozone hole modifies iodine geochemistry on the Antarctic Plateau, Nature Communications, 12, 5836, https://doi.org/10.1038/s41467-021-26109-x, 2021.

Stein, A. F., Draxler, R. R., Rolph, G. D., Stunder, B. J. B., Cohen, M. D., and Ngan, F.: NOAA's HYSPLIT Atmospheric Transport and Dispersion Modeling System, Bulletin of the American Meteorological Society, 96, 2059–2077, https://doi.org/10.1175/BAMS-D-14-00110.1, 2015.

Vicars, W. C. and Savarino, J.: Quantitative constraints on the ^{17}O-excess (Δ^{17}O) signature of surface ozone: Ambient measurements from 50°N to 50°S using the nitrite-coated filter technique, Geochimica et Cosmochimica Acta, 135, 270–287, https://doi.org/10.1016/j.gca.2014.03.023, 2014.

Wang, Y., Choi, Y., Zeng, T., Davis, D., Buhr, M., Gregory Huey, L., and Neff, W.: Assessing the photochemical impact of snow NO_x emissions over Antarctica during ANTCI 2003, Atmospheric Environment, 41, 3944–3958, https://doi.org/10.1016/j.atmosenv.2007.01.056, 2007.

Werle, P., Mücke, R., and Slemr, F.: The limits of signal averaging in atmospheric trace-gas monitoring by Tunable Diode-Laser Absorption Spectroscopy (TDLAS), Applied Physics B Photophysics and Laser Chemistry, 57, 131–139, https://doi.org/10.1007/BF00425997, 1993.

https://doi.org/10.5194/acp-2021-1018
Preprint. Discussion started: 15 December 2021
© Author(s) 2021. CC BY 4.0 License.

Wolff, E. W.: Nitrate in Polar Ice, Ice Core Studies of Global Biogeochemical Cycles, pp. 195–224, https://doi.org/10.1007/978-3-642-51172-1_10, 1995.

Wolff, E. W., Jones, A. E., Bauguitte, S. J.-B., and Salmon, R. A.: The interpretation of spikes and trends in concentration of nitrate in polar ice cores, based on evidence from snow and atmospheric measurements, Atmospheric Chemistry and Physics, 8, 5627–5634, https://doi.org/10.5194/acp-8-5627-2008, 2008.